AD-A141 974 THEORETICAL AND MEASURED AIRFLOW ABOUT THE TWIN OTTER WING (ECOULEMENT AE.. (U) NATIONAL AERONAUTICAL ESTABLISHMENT OTTAWA (ONTARIO) A M DRUMMOND ET AL. 1/1

UNCLASSIFIED MAR 84 NAE-AN-19 NRC-33184 F/G 20/4 NL

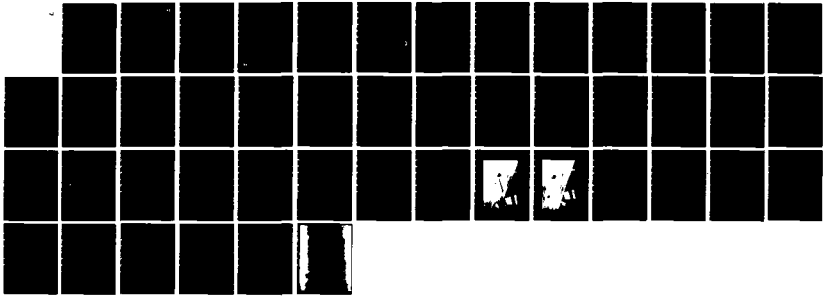

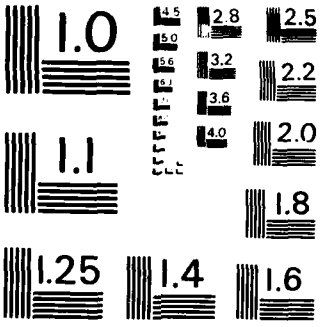

UNLIMITED
UNCLASSIFIED

Canada

6

AD-A141 974

THEORETICAL AND MEASURED AIRFLOW ABOUT THE TWIN OTTER WING

by

A.M. Drummond, J.I. MacPherson

National Aeronautical Establishment

DTIC FILE COPY

OTTAWA
MARCH 1984

AERONAUTICAL NOTE
NAE-AN-19
NRC NO. 33184

National Research Council Canada

Conseil national de recherches Canada

NATIONAL AERONAUTICAL ESTABLISHMENT

SCIENTIFIC AND TECHNICAL PUBLICATIONS

AERONAUTICAL REPORTS:

Aeronautical Reports (LR): Scientific and technical information pertaining to aeronautics considered important, complete, and a lasting contribution to existing knowledge.

Mechanical Engineering Reports (MS): Scientific and technical information pertaining to investigations outside aeronautics considered important, complete, and a lasting contribution to existing knowledge.

AERONAUTICAL NOTES (AN): Information less broad in scope but nevertheless of importance as a contribution to existing knowledge.

LABORATORY TECHNICAL REPORTS (LTR): Information receiving limited distribution because of preliminary data, security classification, proprietary, or other reasons.

Details on the availability of these publications may be obtained from:

Publications Section,
National Research Council Canada,
National Aeronautical Establishment,
Bldg. M-16, Room 204,
Montreal Road,
Ottawa, Ontario
K1A 0R6

ÉTABLISSEMENT AÉRONAUTIQUE NATIONAL

PUBLICATIONS SCIENTIFIQUES ET TECHNIQUES

RAPPORTS D'AÉRONAUTIQUE

Rapports d'aéronautique (LR): Informations scientifiques et techniques touchant l'aéronautique jugées importantes, complètes et durables en termes de contribution aux connaissances actuelles.

Rapports de génie mécanique (MS). Informations scientifiques et techniques sur la recherche externe à l'aéronautique jugées importantes, complètes et durables en termes de contribution aux connaissances actuelles.

CAHIERS D'AÉRONAUTIQUE (AN): Informations de moindre portée mais importantes en termes d'accroissement des connaissances.

RAPPORTS TECHNIQUES DE LABORATOIRE (LTR): Informations peu disséminées pour des raisons d'usage secret, de droit de propriété ou autres ou parce qu'elles constituent des données préliminaires.

Les publications ci-dessus peuvent être obtenues à l'adresse suivante:

Section des publications
Conseil national de recherches Canada
Établissement aéronautique national
Im. M-16, pièce 204
Chemin de Montréal
Ottawa (Ontario)
K1A 0R6

UNLIMITED
UNCLASSIFIED

Canada

AD-A141 974

THEORETICAL AND MEASURED AIRFLOW ABOUT THE TWIN OTTER WING

by

A.M. Drummond, J.I. MacPherson

National Aeronautical Establishment

OTTAWA
MARCH 1984

AERONAUTICAL NOTE
NAE-AN-19
NRC NO. 33184

National Research Council Canada
Conseil national de recherches Canada

NATIONAL AERONAUTICAL ESTABLISHMENT
SCIENTIFIC AND TECHNICAL PUBLICATIONS

AERONAUTICAL REPORTS:

Aeronautical Reports (LR): Scientific and technical information pertaining to aeronautics considered important, complete, and a lasting contribution to existing knowledge.

Mechanical Engineering Reports (MS): Scientific and technical information pertaining to investigations outside aeronautics considered important, complete, and a lasting contribution to existing knowledge.

AERONAUTICAL NOTES (AN): Information less broad in scope but nevertheless of importance as a contribution to existing knowledge.

LABORATORY TECHNICAL REPORTS (LTR): Information receiving limited distribution because of preliminary data, security classification, proprietary, or other reasons.

Details on the availability of these publications may be obtained from:

Publications Section,
National Research Council Canada,
National Aeronautical Establishment,
Bldg. M-16, Room 204,
Montreal Road,
Ottawa, Ontario
K1A 0R6

ÉTABLISSEMENT AÉRONAUTIQUE NATIONAL
PUBLICATIONS SCIENTIFIQUES ET TECHNIQUES

RAPPORTS D'AÉRONAUTIQUE

Rapports d'aéronautique (LR): Informations scientifiques et techniques touchant l'aéronautique jugées importantes, complètes et durables en termes de contribution aux connaissances actuelles.

Rapports de génie mécanique (MS). Informations scientifiques et techniques sur la recherche externe à l'aéronautique jugées importantes, complètes et durables en termes de contribution aux connaissances actuelles.

CAHIERS D'AÉRONAUTIQUE (AN): Informations de moindre portée mais importantes en termes d'accroissement des connaissances.

RAPPORTS TECHNIQUES DE LABORATOIRE (LTR): Informations peu disséminées pour des raisons d'usage secret, de droit de propriété ou autres ou parce qu'elles constituent des données préliminaires.

Les publications ci-dessus peuvent être obtenues à l'adresse suivante:

Section des publications
Conseil national de recherches Canada
Établissement aéronautique national
Im. M-16, pièce 204
Chemin de Montréal
Ottawa (Ontario)
K1A 0R6

UNLIMITED
UNCLASSIFIED

THEORETICAL AND MEASURED AIRFLOW ABOUT THE TWIN OTTER WING

ÉCOULEMENT AÉRODYNAMIQUE THÉORIQUE ET MESURÉ SUR L'AILE DU TWIN OTTER

by/par

A.M. Drummond, J.I. MacPherson

National Aeronautical Establishment

AERONAUTICAL NOTE
NAE-AN-19
NRC NO. 33184

OTTAWA
MARCH 1984

S.R.M. Sinclair, Head/Chef
Flight Research Laboratory/
Laboratoire de recherche en vol

G.M. Lindberg
Director/Directeur

SUMMARY

The NAE Twin Otter atmospheric research aircraft carries instruments mounted under the wings to count and image cloud and precipitation particles for cloud physics studies. As part of an investigation on the influence of the aircraft presence on these measurements, airflow velocities about the wing have been calculated. These theoretical results have been compared with in-flight measurements taken by pressure probes mounted in a cannister suspended from a long and a short pylon below the wing at two spanwise locations.

The Twin Otter wing has been represented by a Joukowski aerofoil of the same maximum thickness but with a cusped trailing edge. The wing camber has been neglected but aspect ratio and planform effects have been included. The effect of the cannister was included in the comparison of theory with experiment. Use of the theory aft of the quarter chord will require experimental verification.

Both experimental and theoretical results for the local flow velocity ratio are linear functions of aircraft lift coefficient (C_L) in the range of C_L between 0.35 to 1.06. The worst discrepancy between theory and experiment in the C_L range of 0.4 to 0.6 is -2.8% to +1.1%. The results for the inboard/long pylon and outboard/short pylon have considerably less deviation.

The theory has been experimentally verified to the above accuracy and can be used to describe the spatial variation of the flow velocity ahead of the wing. Applications of the theory to the study of aircraft flow effects on cloud physics measurements can proceed with a quantifiable level of confidence.

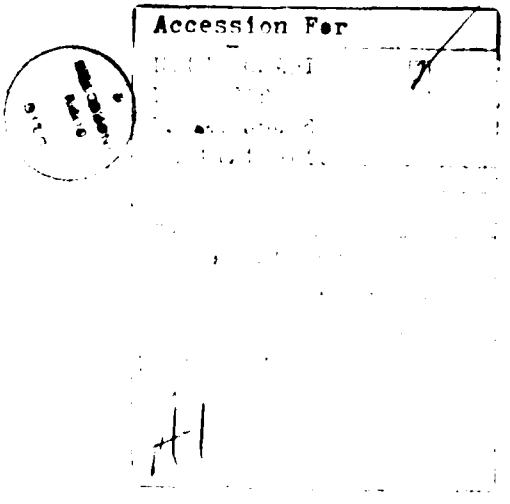

RÉSUMÉ

L'avion Twin Otter pour l'étude de l'atmosphère de l'Établissement aéronautique national transporte sous ses ailes des instruments qui comptent et représentent par une image les particules de nuage et de précipitation pour l'étude de la physique des nuages. Dans le cadre d'une recherche sur l'influence de l'avion sur ces mesures, on a calculé les vitesses de l'écoulement aérodynamique sur les ailes. Ces résultats théoriques ont été comparés à des mesures prises en vol à l'aide de sondes de pression montées sur une boite suspendue par un mât long et par un mât court en deux endroits dans le sens de l'envergure de l'aile.

L'aile du Twin Otter a été représentée par un profil aérodynamique de Joukowski de la même épaisseur maximale, mais comportant un bord de fuite redenté. On n'a pas tenu compte de la courbure de l'aile, mais on a inclus les données des effets de l'allongement et de la forme en plan. On a tenu compte de l'effet produit par la boite dans la comparaison entre la théorie et l'expérimentation. L'application des données théoriques à l'arrière du quart avant doit être effectuée après une comparaison plus approfondie avec les données de l'expérimentation.

Les résultats théoriques et ceux qui découlent de l'expérimentation, en ce qui a trait au rapport de la vitesse d'écoulement local, sont des fonctions linéaires du coefficient de portance (Cz) dans la plage de cette dernière comprise entre 0.35 et 1.06. Le pire écart entre la théorie et l'expérimentation dans la plage de Cz comprise entre 0.4 et 0.6 varie de -2.8% à + 1.1%. Les résultats obtenus pour le mât intérieur long et le mât extérieur court présentent un écart beaucoup moins important.

La théorie a été vérifiée par l'expérimentation au niveau de précision indiqué ci-dessus, et elle peut être employée pour décrire la fluctuation spatiale de la vitesse d'écoulement à l'avant de l'aile. On peut appliquer la théorie à l'étude des effets de l'écoulement sur les mesures en physique des nuages avec une certaine confiance.

CONTENTS

	Page
SUMMARY	(iii)
SYMBOLS	(vii)
INTRODUCTION	1
GEOMETRICAL CONSIDERATIONS	1
MEASUREMENT OF FLOW VELOCITY	6
COMPARISON OF THEORY AND EXPERIMENT	10
CONCLUSIONS	11
REFERENCES	11

TABLES

Table		Page
I	Thickness Parameter Comparisons	2
II	Twin Otter Flight Tests with Airspeed Measuring PMS Cannister	7
III	Deviations from Best Line (Experiment)	9
IV	Intercept Difference	10
V	Slope Comparison	10
VI	Deviation of Theory from Experiment	11

ILLUSTRATIONS

Figure		Page
1	Wing Shape	13
2	Constant Velocity Contours	14
3	Constant Velocity Contours	15
4	Constant Velocity Contours	16
5	Constant Velocity Contours	17
6(a)	Streamlines	18
6(b)	Streamlines	19

ILLUSTRATIONS (Cont'd)

Figure		Page
7(a)	Flow Velocity	20
7(b)	Flow Velocity	21
8(a)	Flow Angle	22
8(b)	Flow Angle	23
9(a)	Long Pylon	24
9(b)	Short Pylon	25
10	Velocity Versus Lift	26
11	Velocity Versus Lift	27
12	Velocity Versus Lift	28
13	Velocity Versus Lift	29

APPENDICES

Appendix		Page
I	A Summary of Theory	31
II	Location of Probe Sample Centers	33

SYMBOLS

Symbol	Definition
a	fundamental length c/4
b	radius of sphere
AR	wing aspect ratio
C_L, C_ℓ	wing, section lift coefficients
c	wing chord
h	conformal transformation
i	$\sqrt{-1}$
L, ℓ	wing, section lift
M	Mach number
m′	compressible wing lift curve slope
m, m_o	wing, section lift curve slopes (incompressible)
n	distance from sphere center
P_T, P_D, P_S	total, dynamic and static pressures
R	gas constant
r	polar co-ordinate in z plane
S	wing area
s	spanwise co-ordinate
T_s	static temperature
t	wing thickness
u, v	velocity in z plane
u_w, v_w	velocity in ζ plane
V_m	measured flow velocity under the wing
V	air speed at infinity
V_s	speed of sound
$\bar{V}$, $\bar{V}_E$	local theoretical, experimental velocity ratios relative to V, $V_{a/c}$, respectively

SYMBOLS (Cont'd)

Symbol	Definition
$V_{a/c}$	aircraft true airspeed
W	aircraft weight
w	complex potential
x, y	co-ordinates in z plane
z	cylinder plane complex variable
z_{ST}	stagnation point
$\bar{\alpha}, \alpha_o$	wing, section angles of attack
α_c	value of α_o at aircraft center
β	camber parameter
γ	ratio of specific heats for air
ρ	air density
τ	wing planform parameter
ϵ	wing thickness parameter
ω	$(\bar{V}-\bar{V}_E)/\bar{V}_E$
ϕ	velocity potential
ψ	stream function
ζ	wing plane complex variable
ξ, η	co-ordinates in wing plane
ξ_1, η_1	co-ordinates for NACA profile
Γ, Γ_c	circulation for a symmetrical, cambered wing
θ	azimuth co-ordinate in z plane

THEORETICAL AND MEASURED AIRFLOW ABOUT THE TWIN OTTER WING

INTRODUCTION

Joukowski aerofoil theory is applied to study the spatial variation of the velocity field in the vicinity of the leading-edge of the Twin Otter wing. The NAE Twin Otter atmospheric research aircraft is instrumented to measure and to compute in real time atmospheric motion and state parameters. For several years it has been used in a cloud physics research role in co-operation with the Atmospheric Environment Service. Particle measuring probes are carried under the aircraft wings to measure cloud droplet spectra, ice particle shapes, etc. These probes are mounted a short distance ahead of cannisters which are suspended by pylons from the wing lower surface. There is evidence to suggest that images and measured concentrations of cloud droplets and ice particles may be affected by the flow around the wings. It was this concern that motivated the initiation of the work described here.

The scope of the report is limited to the establishment of a model for predicting the local flow velocity near the wing as a function of position. Applications of the model to cloud physics will be the subject of another report.

No new theory will be developed here. The results of Glauert (Ref. 1) and Abbot and von Doenhoff (Ref. 2) are used as a theoretical basis. A summary of the theory is given in Appendix I. Kuethe and Schetzer (Ref. 3) have a very clear development of some of the necessary concepts of wing theory that are required in order to apply the two-dimensional results of Glauert.

Glauert (Ref. 1) first published his theory in book form in 1926 and a slightly extended version was published in 1947. He draws upon theory developed in the period 1902-1924. We will refer to his results and quote appropriate page numbers if necessary. Abbot and von Doenhoff (Ref. 2) also rely heavily on the theory of Glauert but their treatment of the subject has exceptional clarity of exposition. Their work was first published in 1949; the 1958 edition quoted here is identical except for a few corrections.

It is clear that the theory being applied here is not new. In this work the full generality of the method is not utilized. The simplest transformation formula is used and wing camber is neglected. The trailing edge of the wing is allowed to be a cusp and no attempt has been made to include the correct trailing edge angle. This latter restriction is thought to be not serious because only flow ahead of the wing quarter-chord point is of interest in the present application.

One of the main contributions of this work is the experimental verification of the method at the locations near the wing where the particle measuring probes are mounted. Without this confirmation, application of the theory would be of academic interest only. Another important result is the linear correlation of the magnitude of the local flow velocity with aircraft lift coefficient in both theoretical and experimental instances.

The next section discusses application of the conformal transformation described in Appendix I to the Twin Otter wing. Some minor extensions to Glauert's results are included.

GEOMETRICAL CONSIDERATIONS

Using Equation (I-5) from the summary of theory in Appendix I, the trailing edge of the wing transforms from 'a' in the z plane to 2a in the ζ plane. In the z plane, the leading edge is located at $-2(a+\epsilon)$ relative to the trailing edge. Hence, the z co-ordinate of the leading edge is $-(a+2\epsilon)$. Using Equation (I-5), the leading edge in the wing plane is located at

$$\zeta_{l.e.} = -(a+2\epsilon) - \frac{a^2}{(a+2\epsilon)}$$

$$= -2a(1+2(\epsilon/a)^2 \ldots) \qquad (1)$$

To first order in ϵ/a, the leading edge is at $\zeta = -2a$. This approximate result shows that the fundamental length of the transformation is very nearly equal to the wing quarter chord. We shall follow Glauert and make the dimension 'a' equal to c/4 correct to about 1%.

The wing shape can be obtained by recognizing that the radius of the circular cylinder is $(a+\epsilon)$ and its center is at $-\epsilon$ (symmetrical wing) on the x axis. The radius from the origin to a point on the cylinder (in the z plane) is:

$$r = a\left\{\epsilon\cos\theta + \sqrt{(\epsilon\cos\theta)^2 + (1+2\epsilon)}\right\} \qquad (2)$$

The co-ordinates in the wing plane in terms of polar co-ordinates in the z plane are

$$\xi = \left(r + \frac{a^2}{r}\right)\cos\theta$$

$$\eta = \left(r - \frac{a^2}{r}\right)\sin\theta \qquad (3)$$

Glauert (Ref. 1, page 75) expands (2) and retains first order terms in ϵ/a. He substitutes the approximate form of (2) in (3), neglects higher order terms, and obtains simple expressions for the wing section co-ordinates ξ and η as functions of θ. He shows that η is a maximum when $\theta = 60°$ and that the thickness-chord ratio of the wing is equal to $3\sqrt{3}\,(\epsilon/4)$ at the quarter chord point. This relation can be used to obtain an approximate estimate of ϵ. For thin wings, the above results are perfectly adequate; however, application of the result to the Twin Otter wing leads to an unduly coarse approximation because its wing is relatively thick (t/c = 0.16).

In this work, the value of ϵ was obtained by a trial and error solution of Equations (2) and (3) to make the maximum value of η equal to half the wing maximum thickness. A trial value of ξ was chosen and the term $\cos\theta$ was taken as the independent variable. In (2), r was calculated and η was obtained from (3). The parameter ϵ was chosen again and the procedure was repeated until the thickness criterion was met. As t/c increases, the approximate solution of Glauert increasingly underestimates the correct value of ϵ. The point of maximum thickness remains at 60°, the quarter chord point.

Table I shows the exact numerical and approximate solutions for ϵ/a at various thickness-chord ratios for a symmetrical wing.

TABLE I

THICKNESS PARAMETER COMPARISONS

t/c	ϵ/a (Glauert)	ϵ/a (exact)
0	0	0
.05	.0385	.0400
.1	.0770	.0830
.15	.1155	.1291
.16	.1232	.1387
.20	.1540	.1782

The Twin Otter wing has an NACA 0016 thickness distribution which is represented analytically by the following equation (Ref. 2, p. 113):

$$\eta_1 = 5(t/c)\left[0.2969\,\xi_1^{1/2} - 0.126\,\xi_1 - .3516\,\xi_1^2 + .2843\,\xi_1^3 - .1015\,\xi_1^4\right] \tag{4}$$

where η_1 and ξ_1 are fractions of the chord c. The thickness at any chordwise location is obtained by doubling the result of (4). Note that with $\xi_1 = 1$. the trailing edge thickness is not zero. Figure 1 shows the Twin Otter wing shape obtained by Equation (4) and the Joukowski aerofoil profile from Equations (2) and (3). The probe locations and the Joukowski parameter values are also shown. There is extremely good agreement between the two shapes as far back as the quarter chord point. The Joukowski profile is slightly fatter than the NACA section until the quarter chord point whereupon the NACA section becomes noticeably thicker. The trailing edge cusp of the Joukowski profile is quite visible.

The stagnation point at the leading edge is located by forcing the terms inside the square brackets in Equation (I-8) to be zero when the value of Γ from Equation (I-9) is inserted. In the z plane, after some lengthy algebra, the result is:

$$z_{ST} = -\left(\epsilon+(a+\epsilon)\cos 2\alpha_o\right) - i(a+\epsilon)\sin 2\alpha_o \tag{5}$$

The stagnation point in the wing plane is obtained by substituting the result of Equation (5) in Equation (I-5). This procedure is best performed numerically. If the approximate forms for the aerofoil co-ordinates due to Glauert are used, one finds that the stagnation point does not lie on the wing. In the present case, it does.

It is apparent that the flow velocity at a given point depends only on α_o and ϵ. The calculation of the thickness parameter ϵ was discussed previously. We now attempt to obtain a value of α_o under the assumptions that the flight speed is not too fast ($M \leqslant .7$) and that the spanwise lift distribution is elliptical. For the Twin Otter, the Mach number restriction is easily met and the lift distribution assumption is approximately fulfilled (Ref. 1, p. 155). The lift at the outboard probe location will be slightly under-estimated but there is no significant discrepancy at the inboard location.

The real wing is describable only by three-dimensional flow while the potential function (Eq. (I-8)) is defined for two-dimensional flow. Kuethe and Schetzer (Ref. 3, p. 96) utilize two-dimensional relations to obtain three-dimensional results for the wing: "The analysis proceeds on the assumption that the flow about each unit span of the finite wing is two-dimensional . . .". We will use the converse statement and obtain two-dimensional values from three-dimensional wing results. The equation for the three-dimensional lift curve slope (m) in terms of the two-dimensional result (m_o) (Ref. 3, p. 100) is:

$$m = \frac{m_o}{1 + \dfrac{m_o}{\pi AR}(1+\tau)} \tag{6}$$

where AR is the wing aspect ratio and τ accounts for planform effects. Values of τ are tabulated (Ref. 1, p. 147) for various values of AR/m_o and taper ratios.

The section lift coefficient C_ℓ is defined as

$$C_\ell = \ell/(\tfrac{1}{2}\rho V^2 c) \tag{7}$$

This can be related to the sectional circulation by the Kutta-Joukowski Theorem (Ref. 2, p. 67) which results after integration:

$$\ell = \rho V \Gamma \tag{8}$$

where the value of Γ is obtained from Equation (I-9). Performing the necessary substitutions and simplifying leads to:

$$C_\ell = 2\pi (1+\epsilon/a) \sin \alpha_o \tag{9}$$

The chord has been taken to be 4a. Differentiating Equation (9) with respect to α_o results in an expression for the two-dimensional lift curve slope for values of α_o small enough to justify the approximation $\cos \alpha_o \cong 1$. The result is:

$$m_o = 2\pi (1+\epsilon/a) \tag{10}$$

Using the value of ϵ/a obtained from Table I at 16% thickness yields the value of m_o as 7.155 per radian. The aspect ratio of the Twin Otter wing is 10. These two numerical values were applied to the data for τ in Reference 1 which allowed the value of τ to be estimated as 0.212.

The three-dimensional lift curve slope can be calculated from Equation (6) using the necessary numerical values. The value of m is 5.607 per radian or .0979 per degree. Elliptic loading requires that the product ($\alpha_o C_\ell c$) must vary elliptically (Ref. 3, p. 99). Therefore, for a rectangular wing with no spanwise thickness variation or twist, the angle of attack α_o must be an elliptical function of the span:

$$\alpha_o(s) = \alpha_c \sqrt{1-s^2} \tag{11}$$

where s is the non-dimensional spanwise co-ordinate and α_c is the value of α_o at the wing center line.

The aircraft C_L is known for a given flight condition. The Prandtl-Glauert rule is applied to m to obtain the lift curve slope m′ when the Mach number is not zero:

$$m' = \frac{m}{\sqrt{1-M^2}} \tag{12}$$

This result is in "remarkably good agreement" (Ref. 2, p. 256) with experimental measurements up to $M \cong .7$.

The average wing angle of attack $\bar{\alpha}$ is obtained from

$$\bar{\alpha} = \frac{C_L}{m'} \tag{13}$$

The value of α_c is chosen to give the same average angle of attack as $\bar{\alpha}$:

$$\alpha_c = \frac{4}{\pi} \bar{\alpha} \tag{14}$$

The local angle of attack α_o is now obtained from Equation (11) at the appropriate spanwise location. The calculation of the velocity field about the wing is now possible.

The Twin Otter wing has a small camber but the details of the shape of the chord line were not readily available. The effect of adding a small amount of camber to a symmetrical wing is to increase the lift coefficient without changing the lift curve slope (Ref. 3, see 18.5).

In fact Glauert (Ref. 1, p. 86) shows that application of the Kutta Condition to a thin wing with small camber results in

$$\Gamma_c = 4\pi a\, V \sin(\alpha_o + \beta) \tag{15}$$

where $\beta = \tan^{-1}$ (2 *camber). If β is negative, the wing is said to be "reflexed". For the Twin Otter, the camber parameter β should be positive and small. The complex potential from Equation (I-6) should be modified to include camber properly.

However, cambered Joukowski aerofoils have circular arcs for their mean chord lines. This shape does not fit the Twin Otter mean chord line very well. Hence, inclusion of camber into the complex potential does not seem to be warranted. Therefore, the effect of camber on the local flow velocity away from the wing is neglected.

In summary, the velocity in the wing plane is obtained from the following equation:

$$\frac{u_w}{V} - i\frac{v_w}{V} = \left[\exp(-i\alpha_o) - \frac{(1+\epsilon/a)^2}{(z/a+\epsilon/a)^2}\exp(i\alpha_o) + i\frac{2(1+\epsilon/a)}{(z/a+\epsilon/a)}\sin(\alpha_o)\right] * \left[\frac{(z/a)^2}{(z/a)^2-1}\right] \tag{16}$$

Equation (I-7) should be used to obtain z for a desired ζ. The magnitude of the local flow velocity relative to the value at infinity is:

$$\bar{V} = \frac{1}{V}\sqrt{u_w^2 + v_w^2} \tag{17}$$

From the previous discussion, after the wing thickness, aspect ratio and planform have been given, the flow velocity depends only on z/a and α_o The latter is determined from the aircraft C_L and to a much lesser extent from the Mach number as well.

For a symmetrical wing at angles of attack small enough for first term approximations to the trigonometric functions to be acceptable, both u_w/V and v_w/V are linear functions of α_o:

$$\frac{u_w}{V} = f_1(x,y)\,\alpha_o$$

$$\frac{v_w}{V} = f_2(x,y)\,\alpha_o$$

Substitution of these results in Equations (16) and (17) and differentiating with respect to α_o shows that $\partial\bar{V}/\partial\alpha_o$ is a constant. The aircraft lift coefficient is a linear function of α_o if compressibility effects are temporarily ignored. Hence, we would expect a plot of $\bar{V}$ versus C_L to be represented very closely by a straight line at low Mach numbers. Computations of $\bar{V}$ versus C_L were performed from Equations (16) and (17). Straight lines fitted the data well for values of α_o below the stall.

The spatial variation of $\bar{V}$ has been calculated for a few values of C_L with compressibility effects being temporarily ignored. All parameters have been chosen to suit the Twin Otter. Lines of constant $\bar{V}$ (isovels) are shown in Figures 2 to 5 for the inboard probe location. The location of the measuring probes at each pylon length under the wing are shown.

As C_L increases, the stagnation point moves farther around the underside of the wing. The isovels are very nearly symmetrical about the leading edge at low C_L.

Consider Figure 4 which shows the isovels at $C_L = 0.55$. Moving from left to right at constant η/a, the velocity variation is markedly different depending on the value of η/a. When the latter variable is -.4 (say) initially one sees $\bar{V}$ slightly less than 1. Moving to the aft limit one encounters a decreasing velocity and then an increasing velocity. The gradients are extremely high near the stagnation point. However, if $\eta/a = -1.4$, the velocity does not change nearly as much and the gradients are much smaller. As C_L increases, velocity decrements are felt farther away from the wing.

The stream function ψ is the imaginary part of the complex potential. It is quite straightforward to calculate the equation for a streamline (ψ = constant) that passes through a given point near the wing. Figures 6(a) and 6(b) show two such lines for high speed and low speed flight respectively that pass through the same point under the wing. The scales of η/a are different. The streamlines are each asymptotic to the appropriate α_o, but near the wing, there is an upwash ahead of the leading edge. The larger the C_L, the larger the upwash. The flow then slopes either down or further up depending on the value of C_L. The streamline to the stagnation point ($\psi = 0$) is shown in each case.

The magnitude of the flow velocity along the streamlines of Figures 6(a) and 6(b) are shown in Figures 7(a) and 7(b). For a low value of C_L, (Fig. 7(a)) the flow velocity is not very different from the flow velocity at infinity. There is a local minimum just ahead of the leading edge. At higher C_L, (Fig. 7(b)), the minimum is more pronounced and occurs a little farther to the rear. The minimum is much lower and the local flow reaches the aircraft speed much farther upstream.

Figures 8(a) and 8(b) show the local flow angle along the same streamlines as in Figures 6(a) and 6(b). In the vicinity of the leading edge, the flow angles exhibit large gradients. There is a local maximum near the leading edge in each case. The lower the value of C_L, the smaller is the change in local flow angle compared to α_o.

MEASUREMENT OF FLOW VELOCITY

A pitot/static and a total pressure probe were installed side-by-side on the nose of a standard Particle Measuring Systems long cannister. Figures 9(a) and 9(b) show this cannister mounted on a short and on a long pylon beneath the Twin Otter wing. The relevant dimensions are given in Appendix II.

It was desired to measure the static pressure (P_S) and dynamic pressure ($P_T - P_S$) ahead of the cannister in the precise sampling plane of a cloud particle measuring probe, but this was not perfectly achievable because of physical limitations in mounting the available pressure probes. Only the static pressure from the pitot/static probe was used. The centre of its two rows of pressure ports, with axial displacement of ½ inch, was ½ inch ahead of the particle sampling plane, and the inlet of the short total pressure probe was ¾ inch aft of this plane. The result is that the static pressure measurements were made at a point 1¼ inches ahead of the total pressure measurements and, on average, ½ inch ahead of the sampling plane. Since static pressure is the critical parameter (P_T should be constant), it is considered to be measured within an acceptable dimensional tolerance (0.3% of chord); hence, its measurements can be considered to apply at the sampling plane. The 2 inch lateral separation between the static and the total pressure probes can be ignored, because there is negligible spanwise variation in the flow about the constant section wing of the Twin Otter at the probe mounting locations.

Static and dynamic pressure transducers were housed within the cannister. The transducers had very short pressure lines to the probes. The dynamic pressure was measured differentially between the total head probe (P_T) and the static pressure (P_S) from the pitot/static probe. Signals from the transducers were carefully calibrated and recorded digitally at 16 samples/second on the NAE recording system along with all the other parameters normally recorded on the Twin Otter (Ref. 7). The recording resolutions for P_S and $P_T - P_S$ were 0.97 and .07 millibars per bit respectively, while RMS errors in the quadratic fits to the calibrations were 0.73 and .02 millibars.

Four test flight configurations were flown. The airspeed measuring cannister was mounted on both short and long pylons, and at both the inboard and outboard positions on the wing. Stabilized level flight was selected at several altitudes over a range of indicated airspeeds from near the flaps-up stall speed to near full speed at about 10 knot increments. For each test run the event marker on the recording system was depressed for about 10 seconds to denote a valid stabilized flight condition. During the subsequent analysis, data were averaged over this period. For at least one altitude on each flight, runs were flown in both an increasing and decreasing order of speeds to ensure that there were no measurement errors due to hysteresis. Differing fuel loads were carried to cover the usual operating gross weight range of the aircraft. Table II presents the test points flown over the following wide range of flight parameters:

(i) indicated airspeeds from 80 to 140 knots (41 to 72 m s^{-1})
(ii) altitude from 4000 to 9500 feet
(iii) air temperatures from -1 to 20°C
(iv) true airspeeds from 93 to 167 knots (48 to 86 m s^{-1})
(v) aircraft weight from 9800 to 11400 lbs. (maximum gross weight is 11579 lbs.).

TABLE II

TWIN OTTER FLIGHT TESTS WITH AIRSPEED MEASURING PMS CANNISTER

Spanwise Position	Pylon Length	Altitude Feet	Airspeed Range kt IAS	Aircraft Weight lb.
Inboard	Long	4000	80 — 140	9800 — 11400
		6000	135 — 80	
			120 — 80	
		8200	140 — 80	
		9500	80 — 135	
	Short	6000	135 — 80	10570 — 10770
		7000	85 — 125	
		9500	130 — 80	
			85 — 125	
Outboard	Long	6000	135 — 80	10450 — 10630
		7000	85 — 135	
		9500	135 — 80	
			85 — 135	
	Short	6000	135 — 80	10340 — 10575
			85 — 135	
		9500	130 — 80	
			85 — 130	

The local flow velocity was determined by using the perfect gas law and isentropic flow equations (Ref. 5). In particular, the local Mach number (M) was obtained from measured total and static pressures by utilizing the relation:

$$P_T = P_S \left(1 + \frac{\gamma - 1}{2} M^2\right)^{\frac{\gamma}{(\gamma-1)}} \tag{18}$$

where γ is the ratio of specific heats for air (1.4).

The speed of sound (V_s) was calculated from the measured static temperature (T_s) by the equation

$$V_s = \sqrt{\gamma R T_s} \tag{19}$$

where R is the universal gas constant. Humidity effects have been ignored in this calculation of the speed of sound. The local flow velocity V_m was obtained by multiplying the Mach number by the speed of sound

$$V_m = V_s M \tag{20}$$

The aircraft lift coefficient is defined as

$$C_L = W/(\tfrac{1}{2}\rho V_{a/c}^2 S) \tag{21}$$

where S is the wing area (420 ft.^{2}). The measured value of T_s and the perfect gas law were used to obtain the air density ρ. Aircraft true airspeed derived from the nose boom pitot/static system was computed by the real-time microprocessor and was recorded on the NAE recorder. Aircraft weight was carefully deduced for each test point by taking account of fuel used and aircraft weight at take-off. The definition in Equation (21) requires steady level flight; however, some data were taken in light turbulence which may account for some of the scatter in the experimental values.

The total pressure from the nose boom was computed from the sum of the recorded static and dynamic pressures. The total pressure from the wing-mounted probe was consistently 1 to 2 mb higher than the nose measurement. This small systematic error is probably due to an error in the calibration of the nose boom static pressure transducer; however, the resulting errors in Mach number and aircraft true airspeed are negligible.

The variable $\bar{V}_E$ is defined:

$$\bar{V}_E = V_m / V_{a/c} \tag{22}$$

It was calculated for each test point as the ratio of the velocity at the probe to the aircraft true airspeed. The lift coefficient was calculated from Equation (21).

The results are plotted in the form of V_E versus aircraft C_L in Figures 10 to 13 for the two pylon lengths and the two spanwise cannister locations. A least-squares procedure was used to fit a straight line to the measured data and the line is plotted (dashed line) on the Figures. The measured velocity ratios were well described by the straight line in each case. Table III shows maximum deviations of measured points from the straight line.

TABLE III

DEVIATIONS FROM BEST LINE (EXPERIMENT)

Figure	Span	Pylon	Maximum Deviation %
10	Inboard	Long	± 3/4
11	Inboard	Short	± 1/2 (except near $C_L = 1$)
12	Outboard	Long	± 1/2
13	Outboard	Short	+ 1-1/8, -7/8

Symbols on the graphs correspond to data taken at different nominal altitudes and aircraft weights. There is clearly no orderly variation of the results with altitude. Hence, no further identification of the symbols was thought to be necessary.

Cannister Effects

Normally, the flow about an aggregate of bodies is obtained by summing the complex potentials of all the bodies. If one body (the cannister) is very much smaller than the other (the wing), then velocity gradients due to flow about the larger body may be extremely small on length scales of the smaller body. The cannister can be considered to be in a uniform flow whose magnitude and direction depend only on the position of the cannister with respect to the wing.

The velocity measuring pressure probes are mounted on long cylindrical cannisters with hemispherical ends. The length to diameter ratio is about 9 which allows the application of slender body theory to the discussion of flow effects of the cannister. This is necessary because the measurements were taken in a region where the flow is affected by the cannister.

The local flow at the nose of the cannister is decomposed into an axial component ($V\cos\alpha_0$) and a cross-flow component ($V\sin\alpha_0$). The latter causes viscous separation on the probe body but the axial component is assumed to be unaffected. Potential flow is assumed for the axial flow. It is sufficient to allow the approximation $\cos\alpha_0 \approx 1$ in the present case because the local flow angles are small.

The dominant effect of the cannister is due to the blunt nose, which we shall model as a sphere. There will be some alleviation of velocity decrements near the probe nose because of the cylindrical after-body but these will be neglected. The velocity field near a sphere of radius b (Ref. 6, p. 443) looking directly along the velocity vector V is:

$$u = V\left[1 - \left(\frac{b}{n}\right)^3\right] \tag{23}$$

where n is the distance from the sphere center to the point of interest.

Velocity decrements at the measurement point are easily calculated by noting that the radius of the sphere is 3.25 inches and that the measurements of static pressure are taken at a point 6-5/16 inches in front of the nose of the cannister. At that point,

$$u = .9607V \tag{24}$$

which means that $\bar{V}$ from the wing calculations must be multiplied by .9607 to be comparable to the measured values $\bar{V}_I$. This procedure was employed for the following comparison of theoretical and experimental velocity ratios.

COMPARISON OF THEORY AND EXPERIMENT

At the measured C_L, the theoretical velocity ratio was calculated from Equation (16) using the previously noted procedure to obtain α_0 and it was corrected for cannister effects by Equation (24). A straight line of $\bar{V}$ versus C_L was obtained in the C_L range from 0.35 to 1.05. The theoretical result corrected for cannister effects is shown on Figures 10 to 13 as a dotted line. Values of $\bar{V}$ at C_L of 0.3, 0.6 and 0.9 were calculated. In all cases, a straight line could be drawn through the calculated points. The least squares fit to the experimental data and each measured point are shown on the same figures for comparison.

Table IV shows the difference between the intercepts for the theoretical and experimental straight lines.

TABLE IV

INTERCEPT DIFFERENCE

Span	Pylon	Theory-Experiment
Outboard	Long	.0073
	Short	.0134
Inboard	Long	.0031
	Short	.0071

Table V shows the same comparison for the slopes of the theoretical and experimental straight lines:

TABLE V

SLOPE COMPARISON

Span	Pylon	Theory	Experiment
Outboard	Long	-.2963	-.3004
	Short	-.3640	-.3461
Inboard	Long	-.3464	-.3264
	Short	-.4305	-.3863

The intercept of the theoretical line is very slightly larger than that of the experimental line and the magnitude of the slope of the theoretical line is also slightly larger in 3 out of the 4 cases. Cloud penetration by the aircraft typically occurs at an aircraft C_L between 0.4 and 0.6 for the Twin Otter. In all cases, the agreement between theory and experiment is good in this range. The results for the inboard pylon location are under-estimated by the theory while the measurements for the outboard location are over-estimated by the theory.

It is not possible to isolate reasons for disagreement between theory and experiment. Even though the experimental results are subject to error, it is fair to attribute discrepancies to the theoretical model. Some physical variables were ignored (trailing edge angle, camber and aircraft thrust effects on C_L). However in the C_L range of 0.4 to 0.6, the experimental results are well-predicted by the theory with the accuracy shown in Table VI, where

$$\omega = (\bar{V} - \bar{V}_{L'})/\bar{V}_{L'} \tag{25}$$

TABLE VI

DEVIATION OF THEORY FROM EXPERIMENT

Span	Pylon	C_L	ω %
Inboard	Long	.4	- .52
		.6	-1.02
Inboard	Short	.4	-1.67
		.6	-2.82
Outboard	Long	.4	+ .97
		.6	+1.10
Outboard	Short	.4	+ .65
		.6	+ .30

These data in Table VI show that the theory as presented here has been verified with sufficient accuracy. Its application can be extended to the study of spatial variation of local flow velocity in regions ahead of the points at which measurements were made. The theory can be used in choosing the best location to mount instrumentation that is affected by airflow.

CONCLUSIONS

The Twin Otter wing has been represented by a Joukowski aerofoil of the same maximum thickness but with a cusped trailing edge. The wing camber has been neglected but aspect ratio and planform effects have been included. The effect of the cannister was included in the comparison of theory and experiment. Application of the theory aft of the quarter chord will require more experimental data.

Both experimental and theoretical results for the local flow velocity ratio are linear functions of aircraft C_L in the range of C_L between 0.35 to 1.06. The worst discrepancy between theory and experiment in the C_L range of 0.4 to 0.6 is -2.8% to +1.1%. The results for the inboard/long pylon and outboard/short pylon have considerably less deviation.

The theory has been experimentally verified to the above accuracy and can be used to describe the spatial variation of the flow velocity ahead of the wing. Applications of the theory to the study of aircraft flow effects on cloud physics measurements can proceed with a quantifiable level of confidence.

REFERENCES

1. Glauert, H. *The Elements of Aerofoil and Airscrew Theory.* Second edition, Cambridge University Press, 1947.

2. Abbot, I.H. and von Doenhoff, A.E. *Theory of Wing Sections.* Dover Publication, 1958.

3. Kuethe, A.M. Schetzer, J.D. *Foundations of Aerodynamics.* Wiley and Sons, 1950.

4. Hildebrand, F.B. *Advanced Calculus for Engineers.* Prentice-Hall, 1949.

5. Liepmann, H.W. Roshko, A. *Elements of Gas Dynamics.* Wiley and Sons, 1957.

6. Milne-Thomson, L.M. *Theoretical Hydrodynamics.* 2nd edition, MacMillan, 1952.

7. MacPherson, J.I. Morgan, J.M. Lum, K. *The NAE Twin Otter Atmospheric Research Aircraft.* NRC, NAE Laboratory Technical Report LTR-FR-80, National Research Council, March 1981.

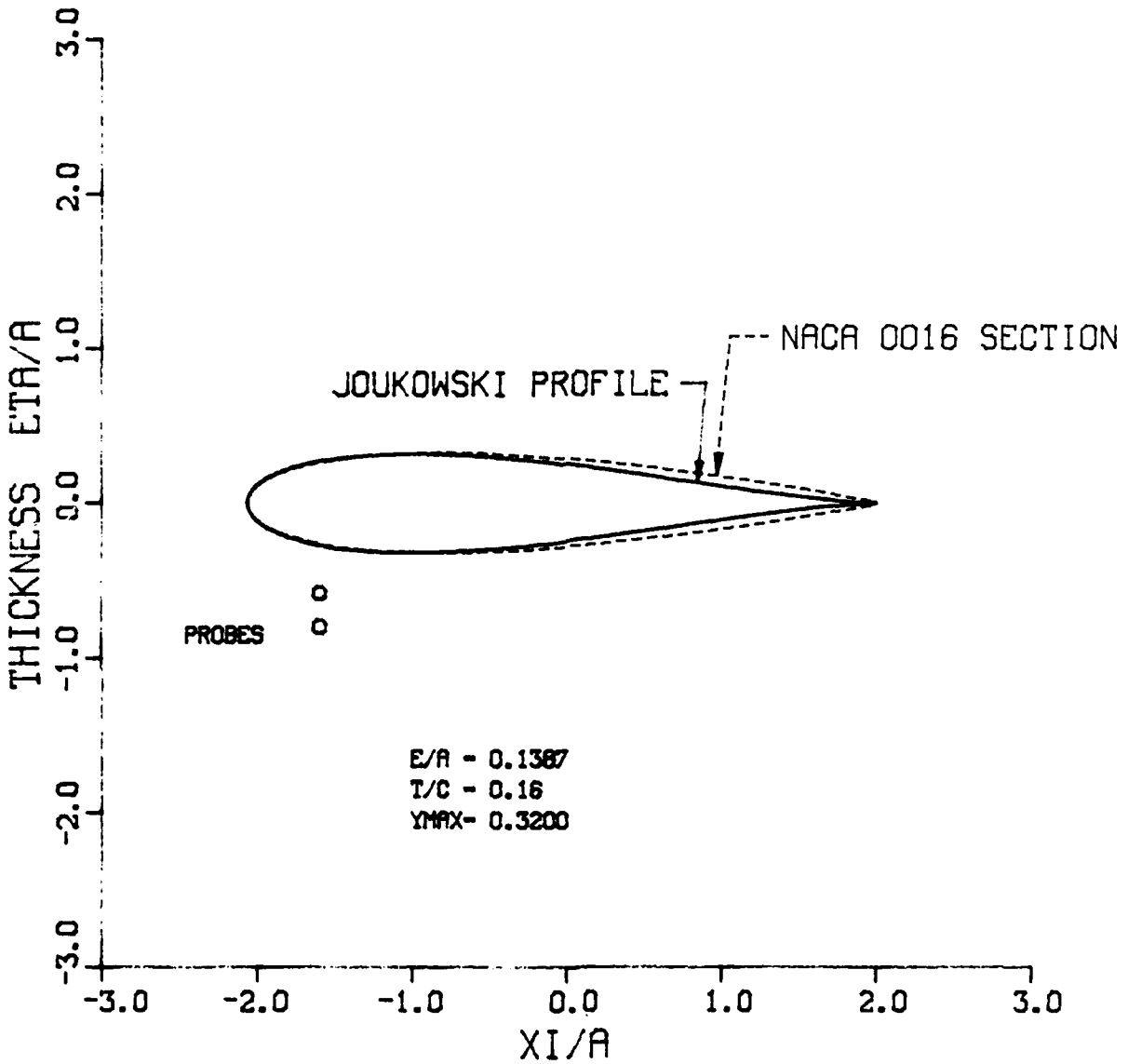

FIG. 1: WING SHAPE

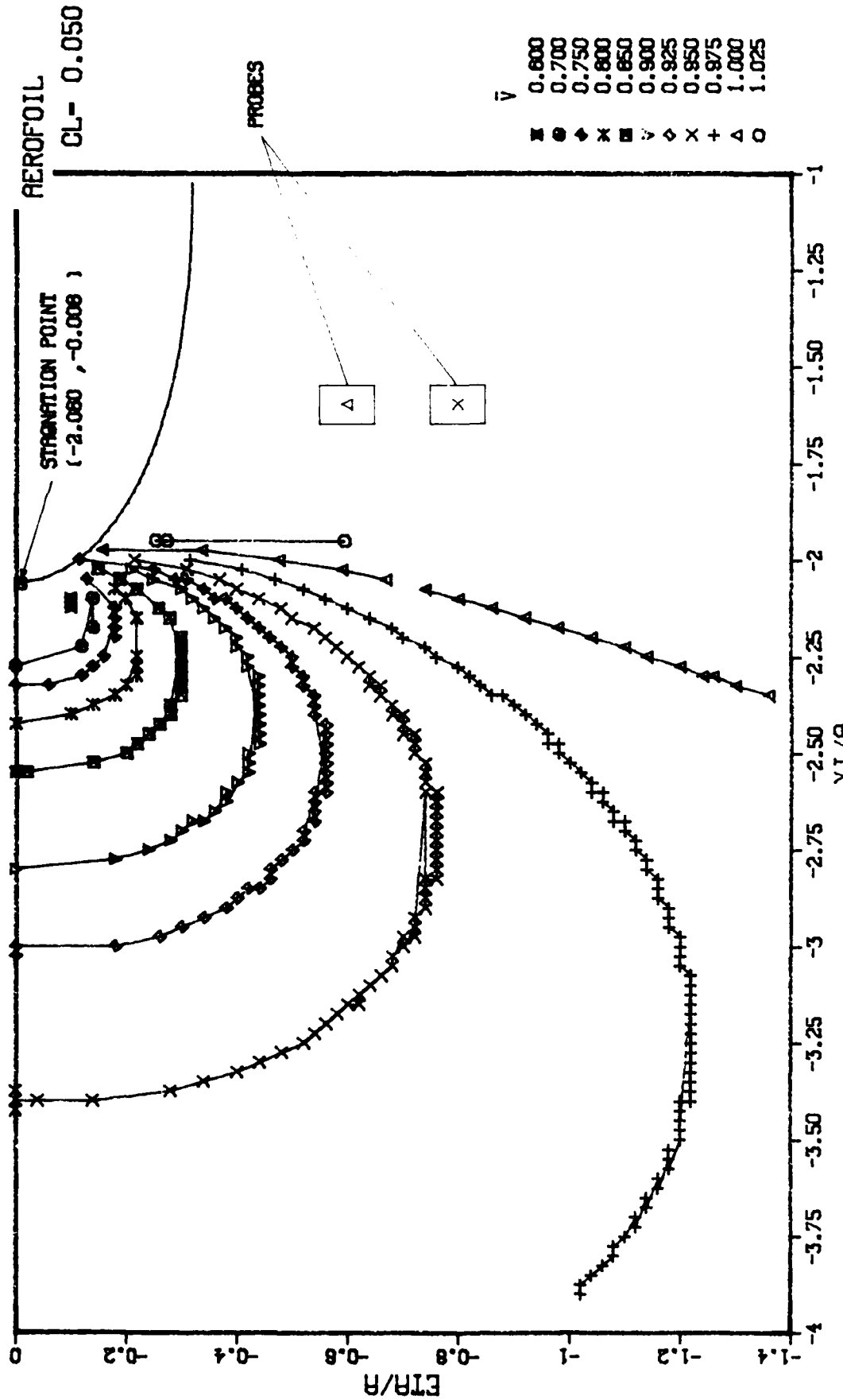

FIG. 2: CONSTANT VELOCITY CONTOURS

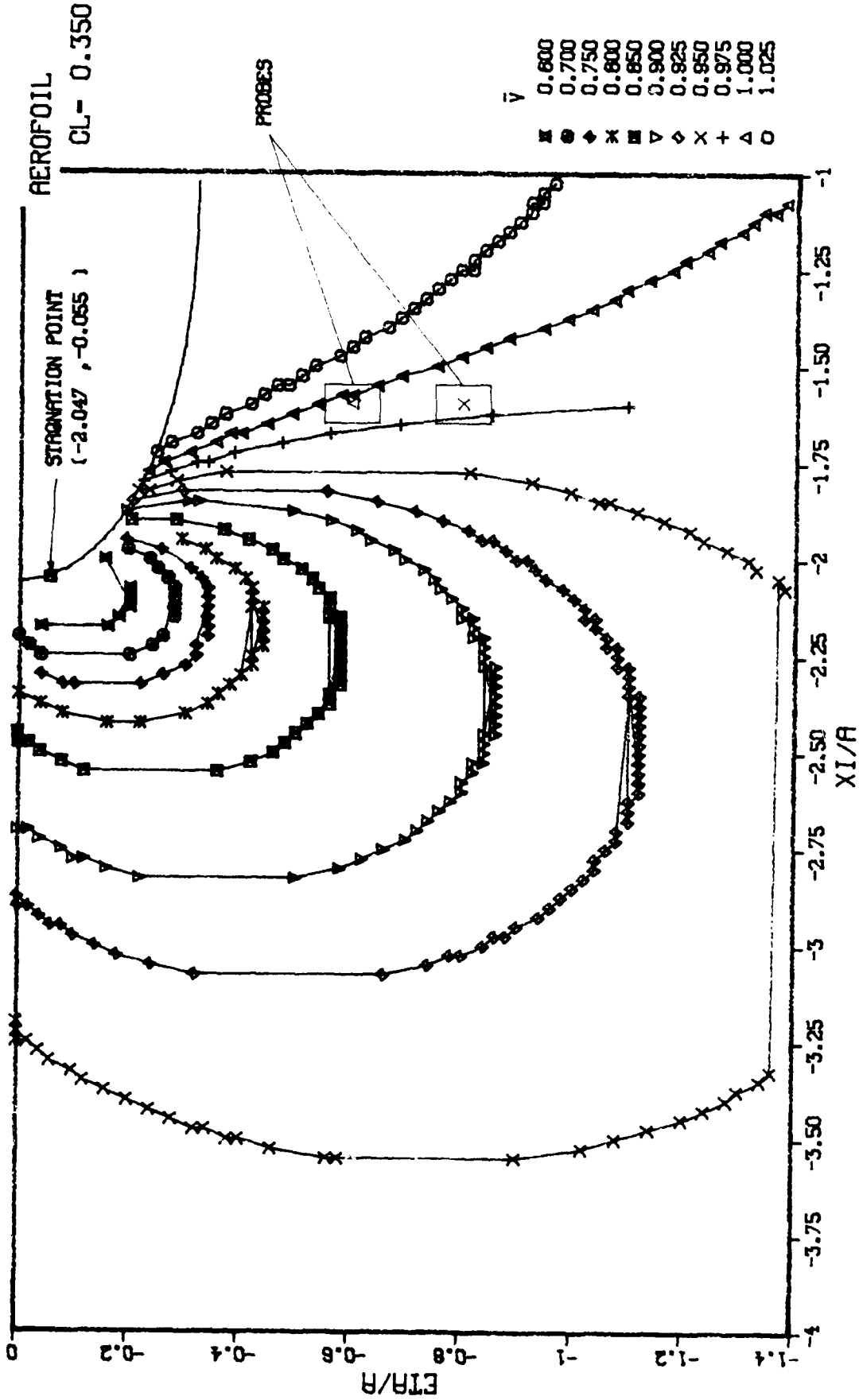

FIG. 3: CONSTANT VELOCITY CONTOURS

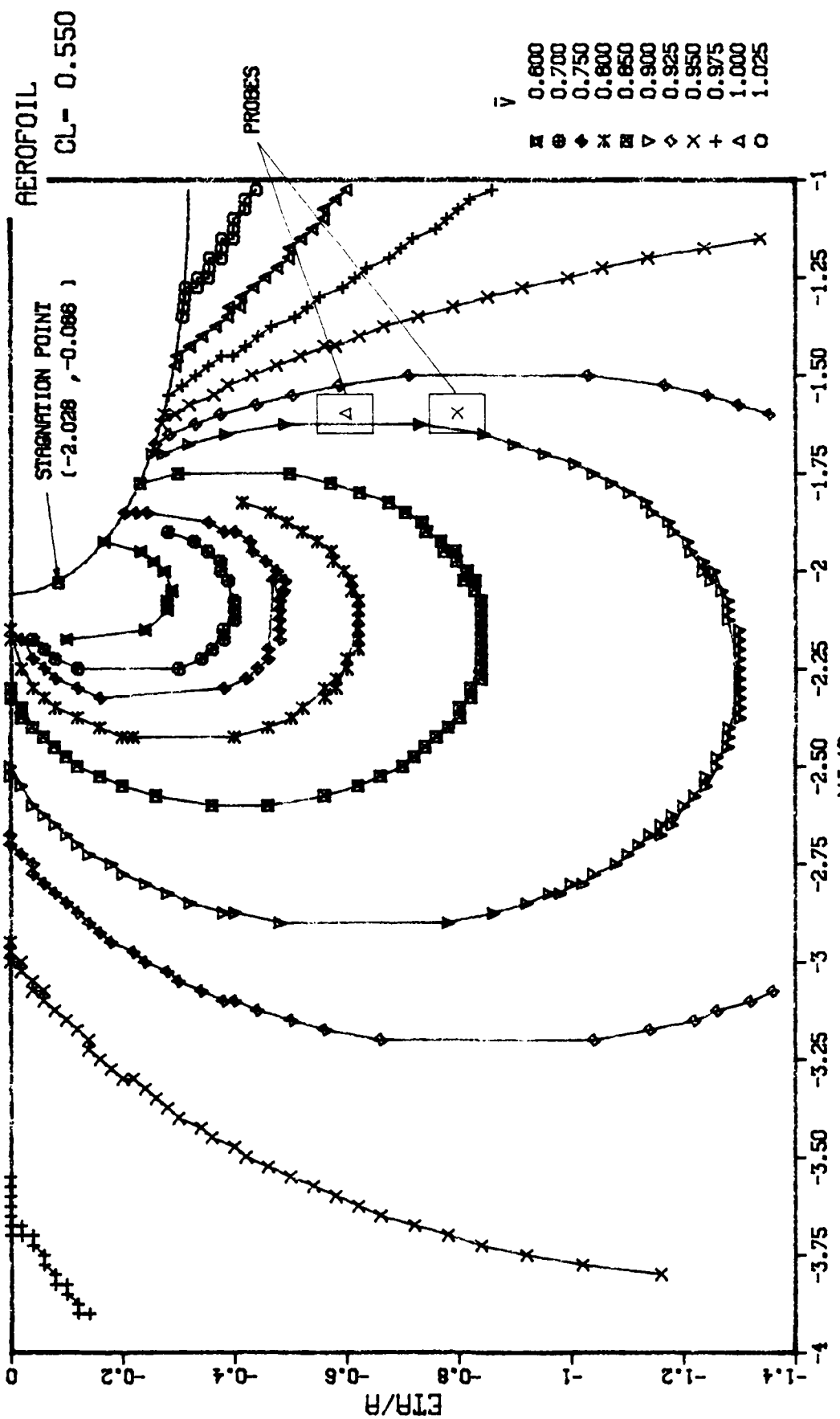

FIG. 4: CONSTANT VELOCITY CONTOURS

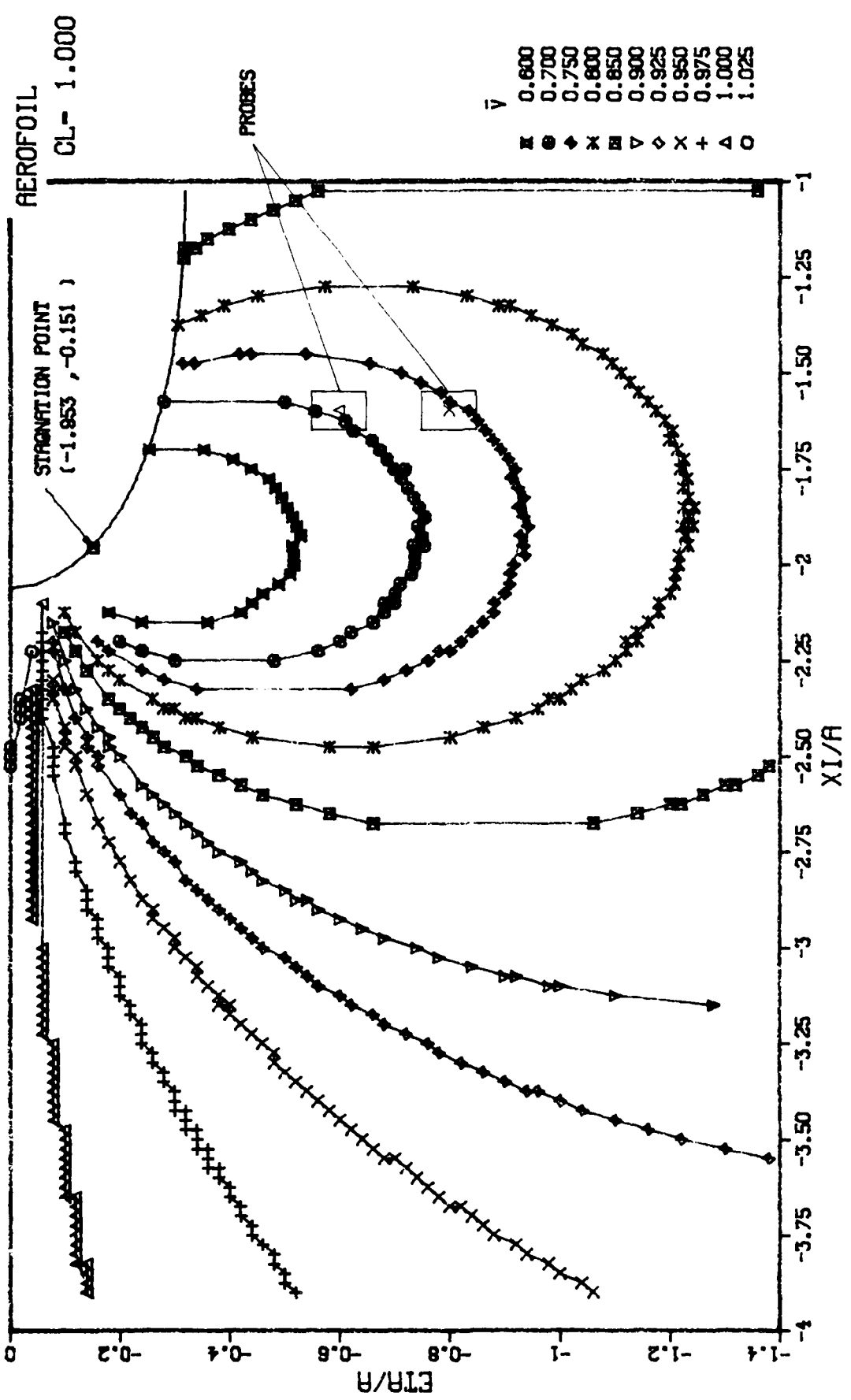

FIG. 5: CONSTANT VELOCITY CONTOURS

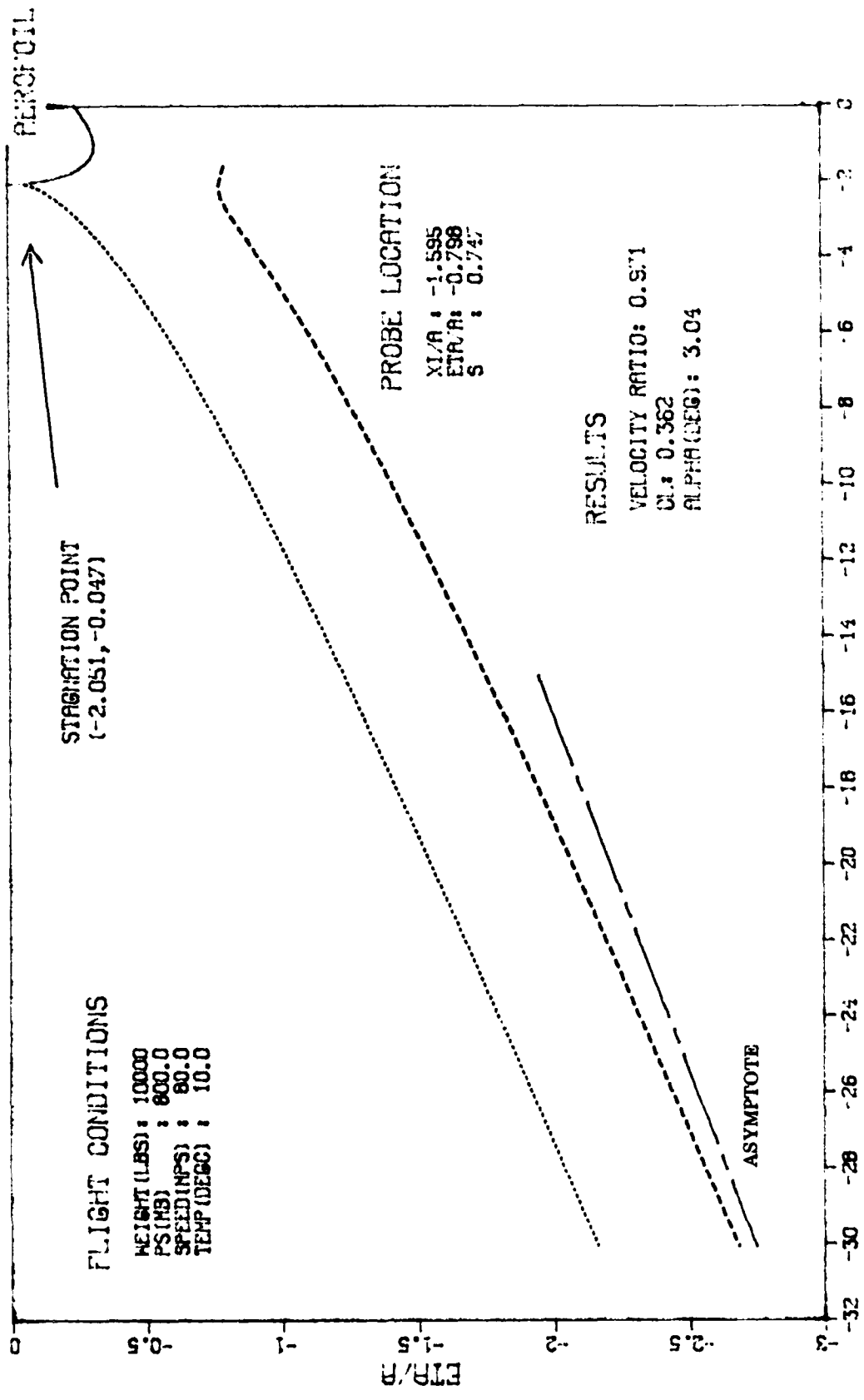

FIG. 6(a): STREAMLINES

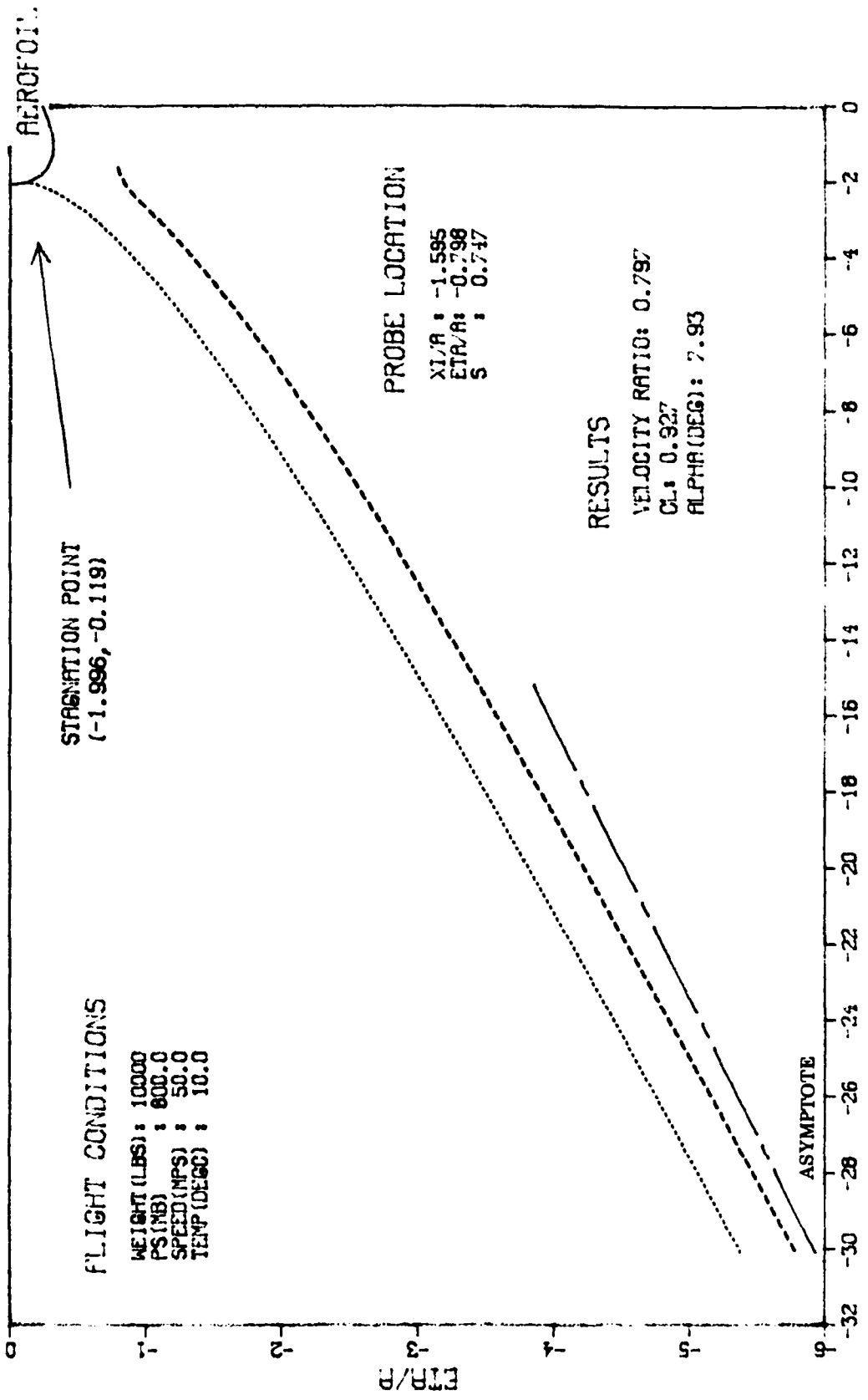

FIG. 6(b): STREAMLINES

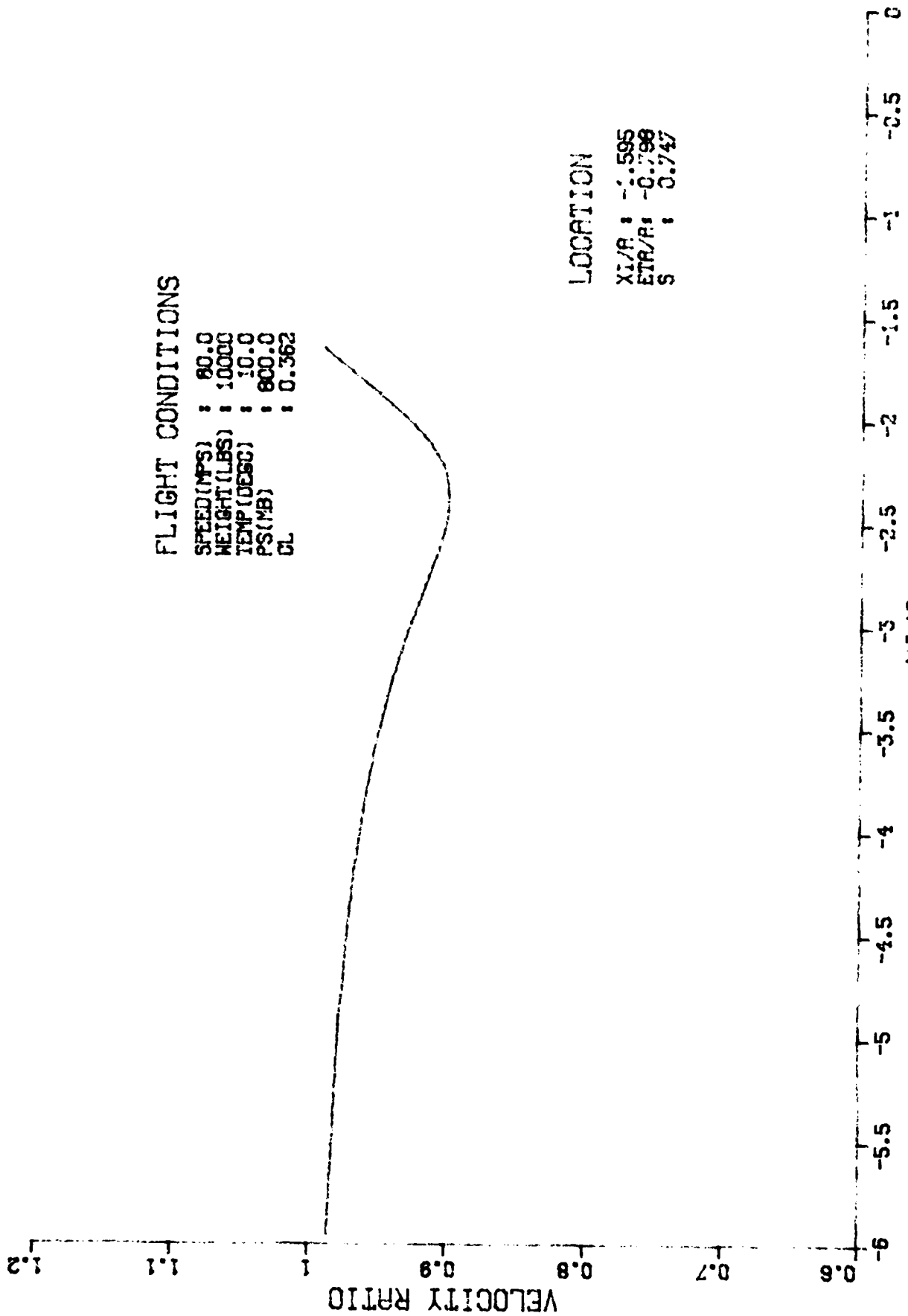

FIG. 7(a): FLOW VELOCITY

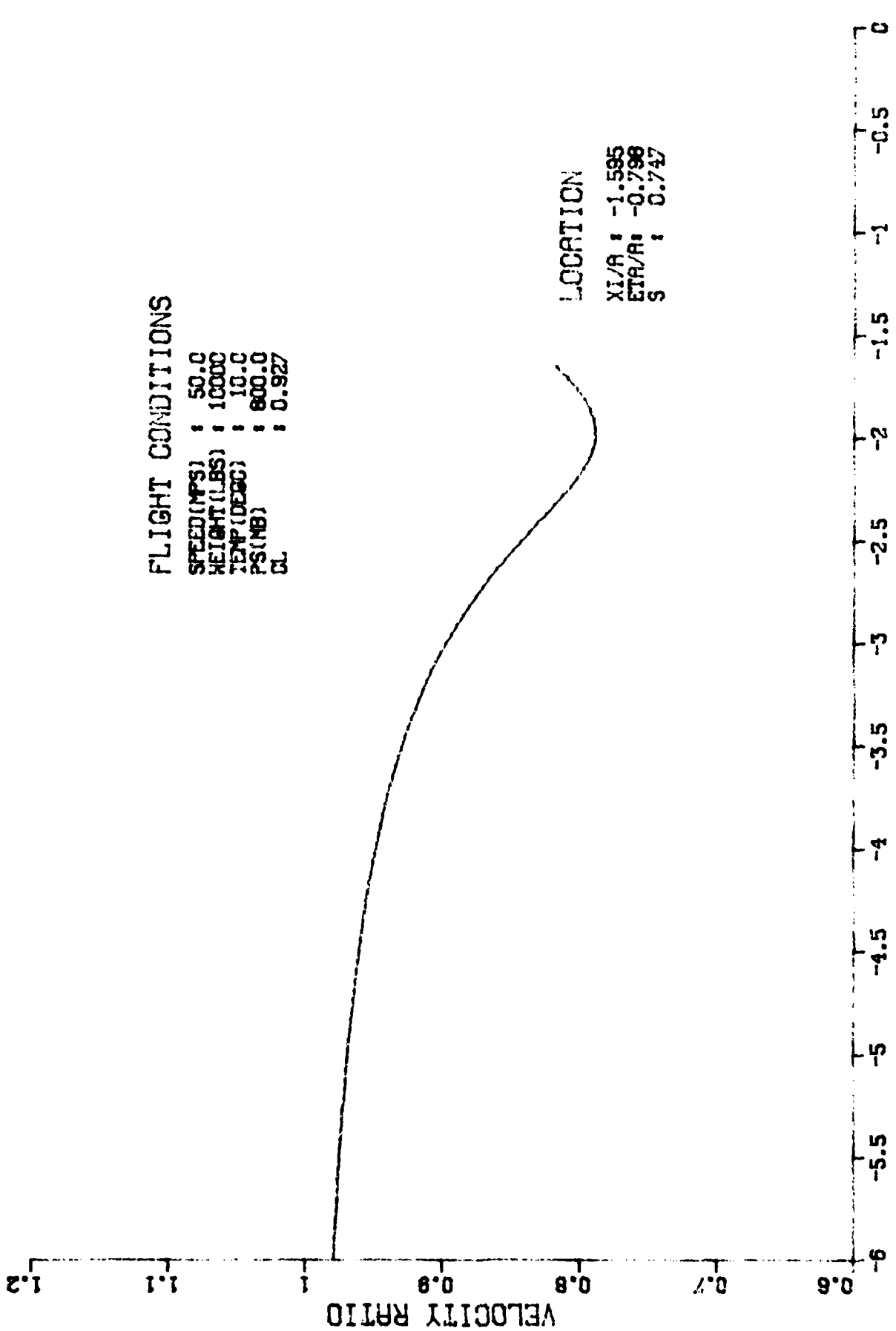

FIG. 7(b): FLOW VELOCITY

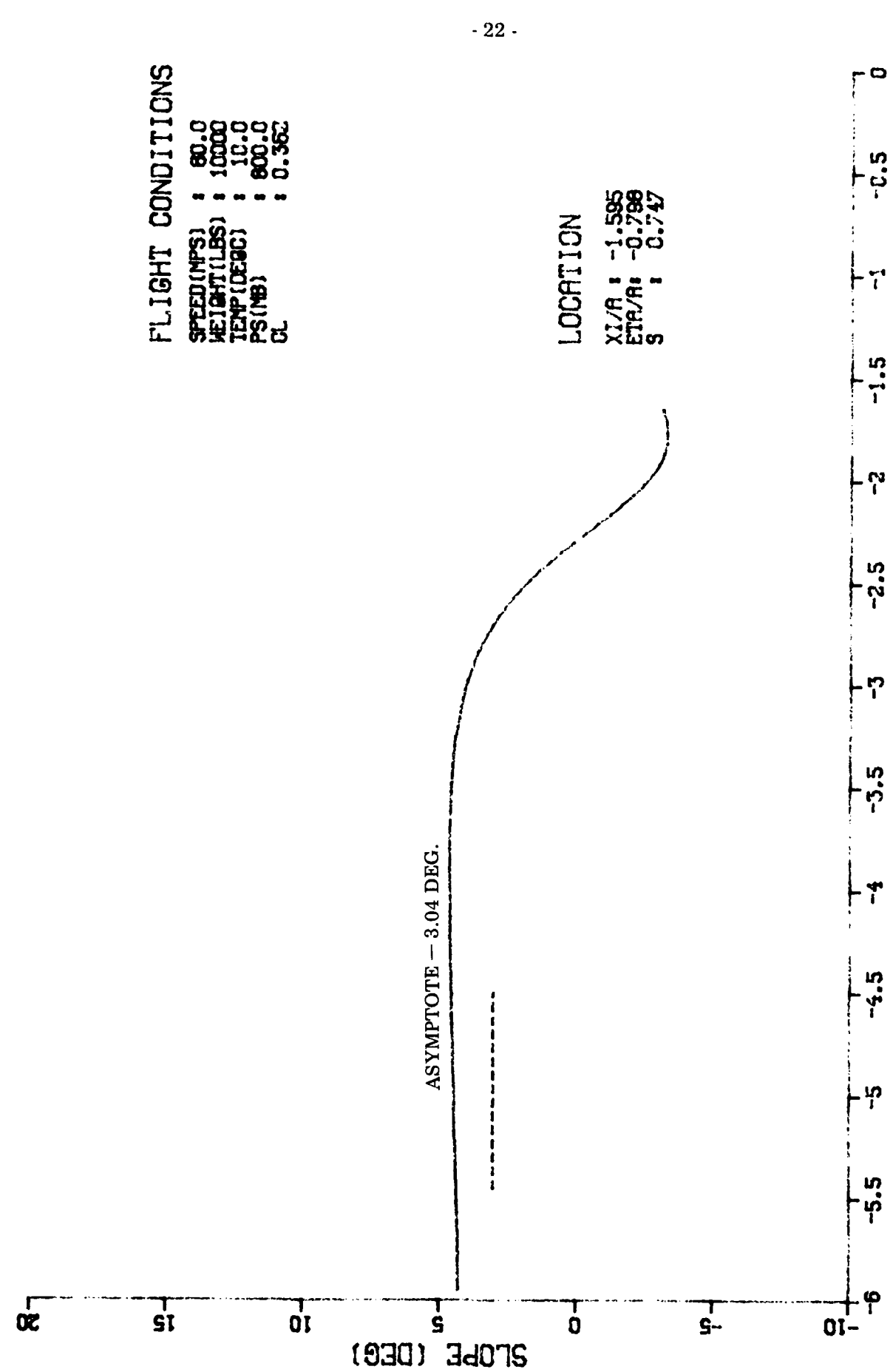

FIG. 8(a): FLOW ANGLE

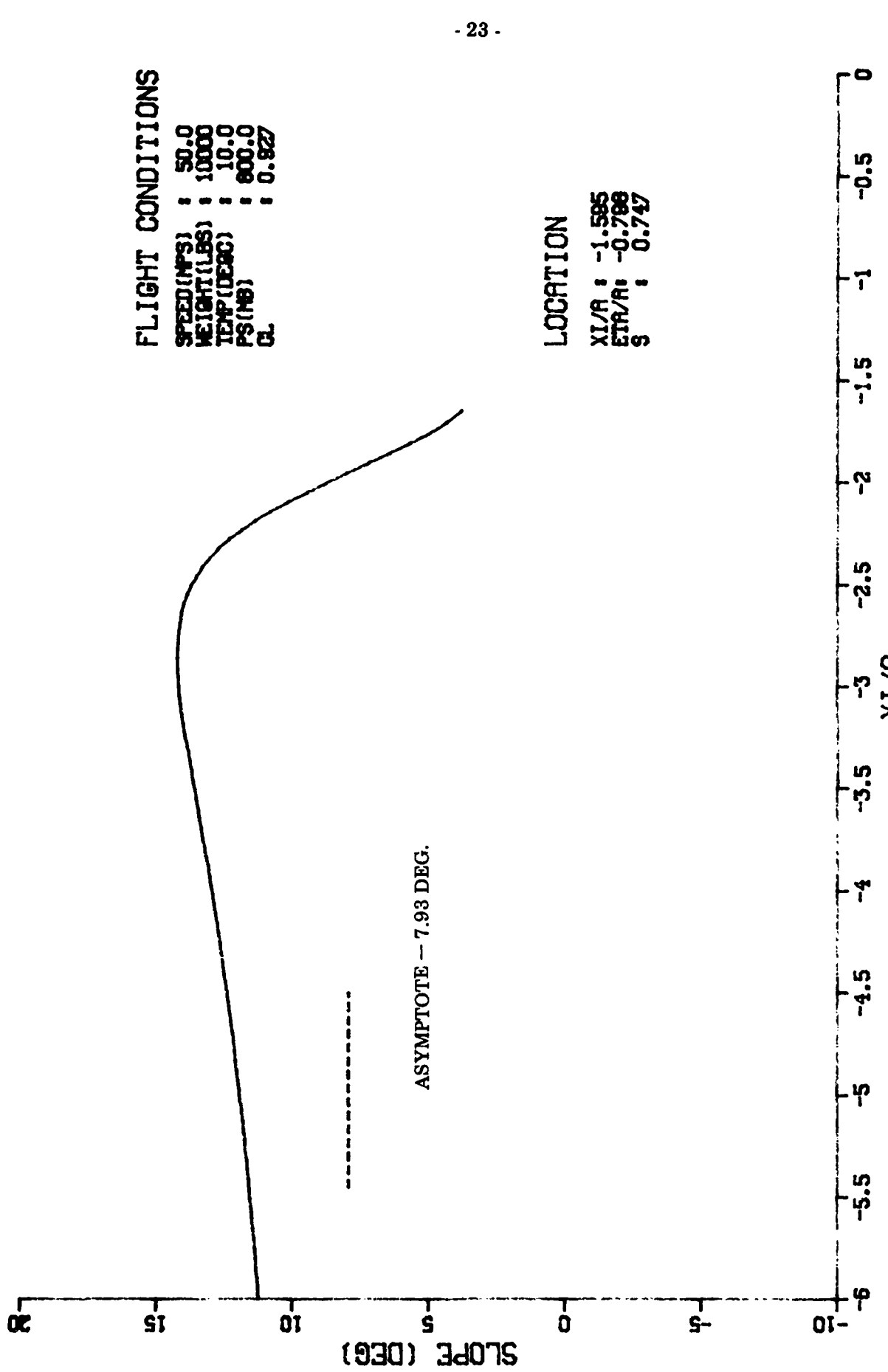

FIG. 8(b): FLOW ANGLE

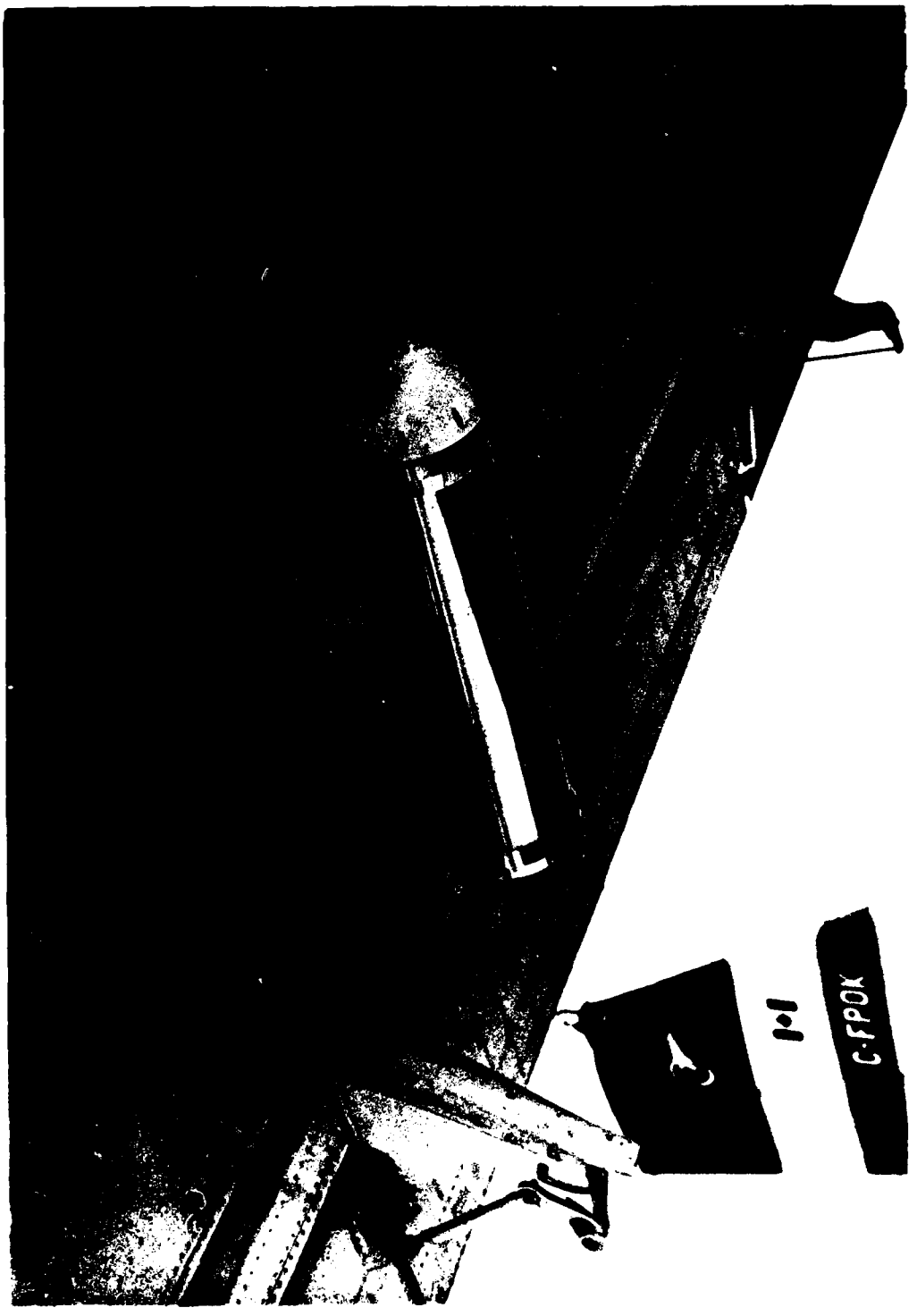

FIG. 9(a): LONG PYLON

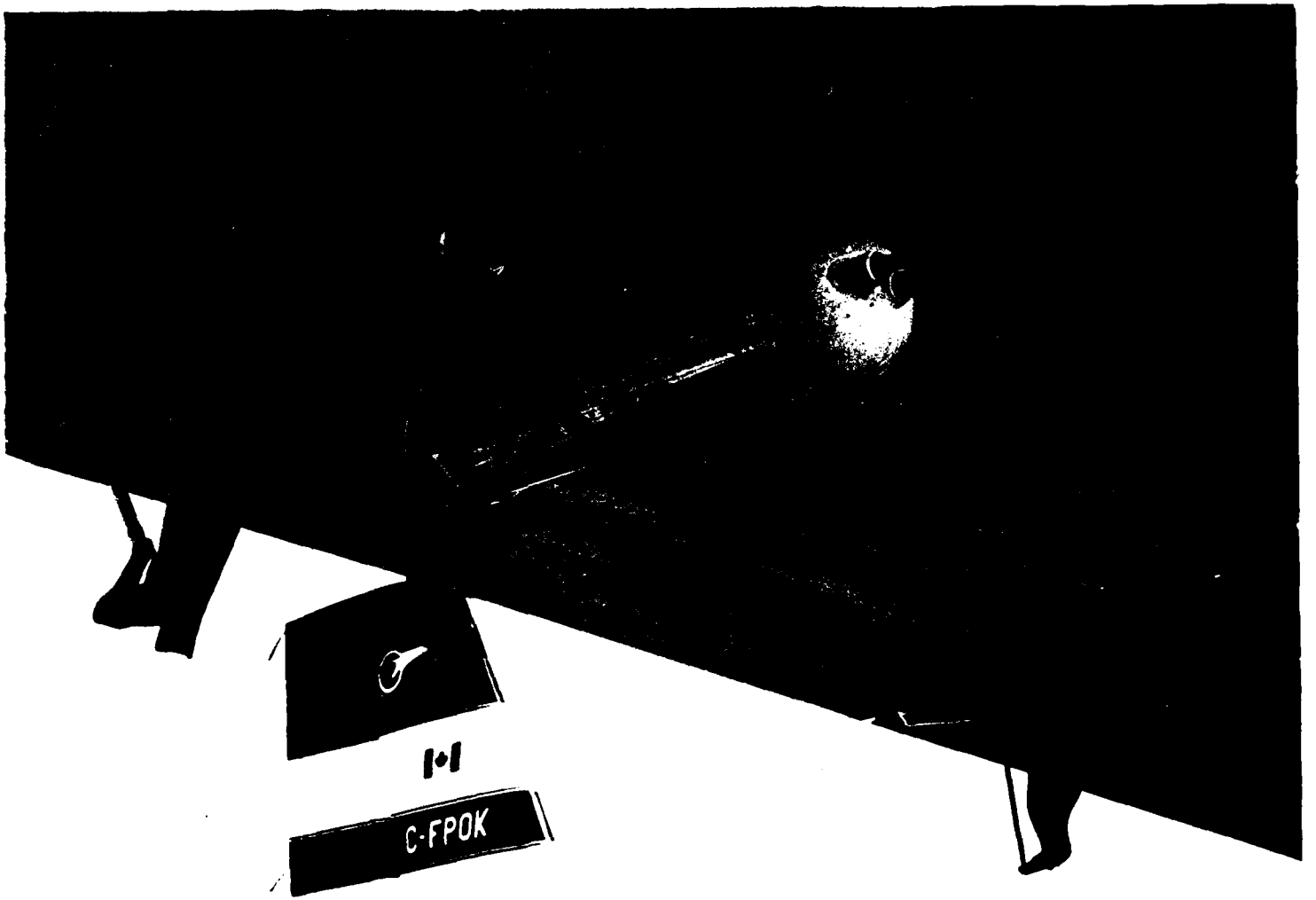

FIG. 9(b): SHORT PYLON

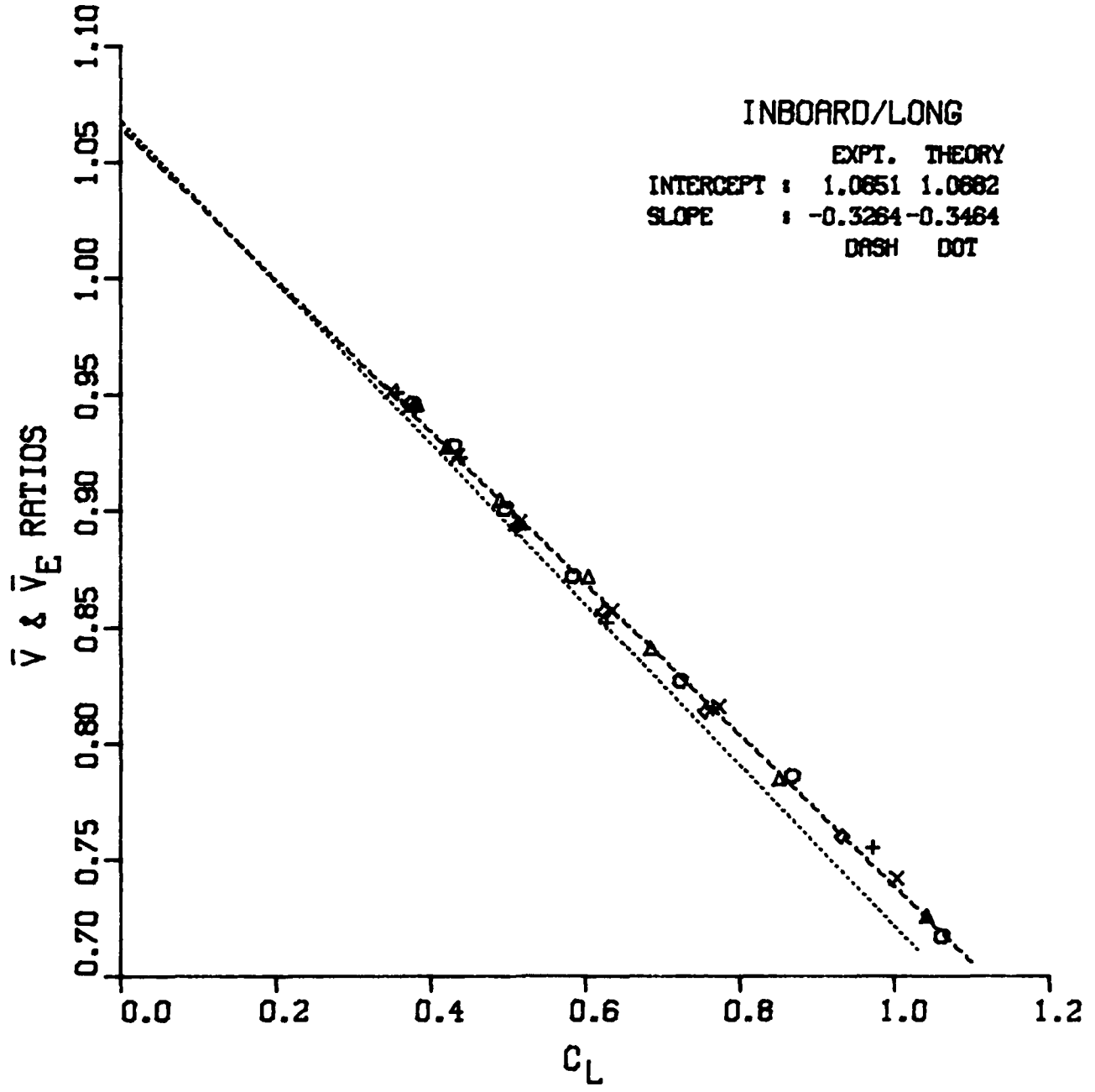

FIG. 10: VELOCITY VERSUS LIFT

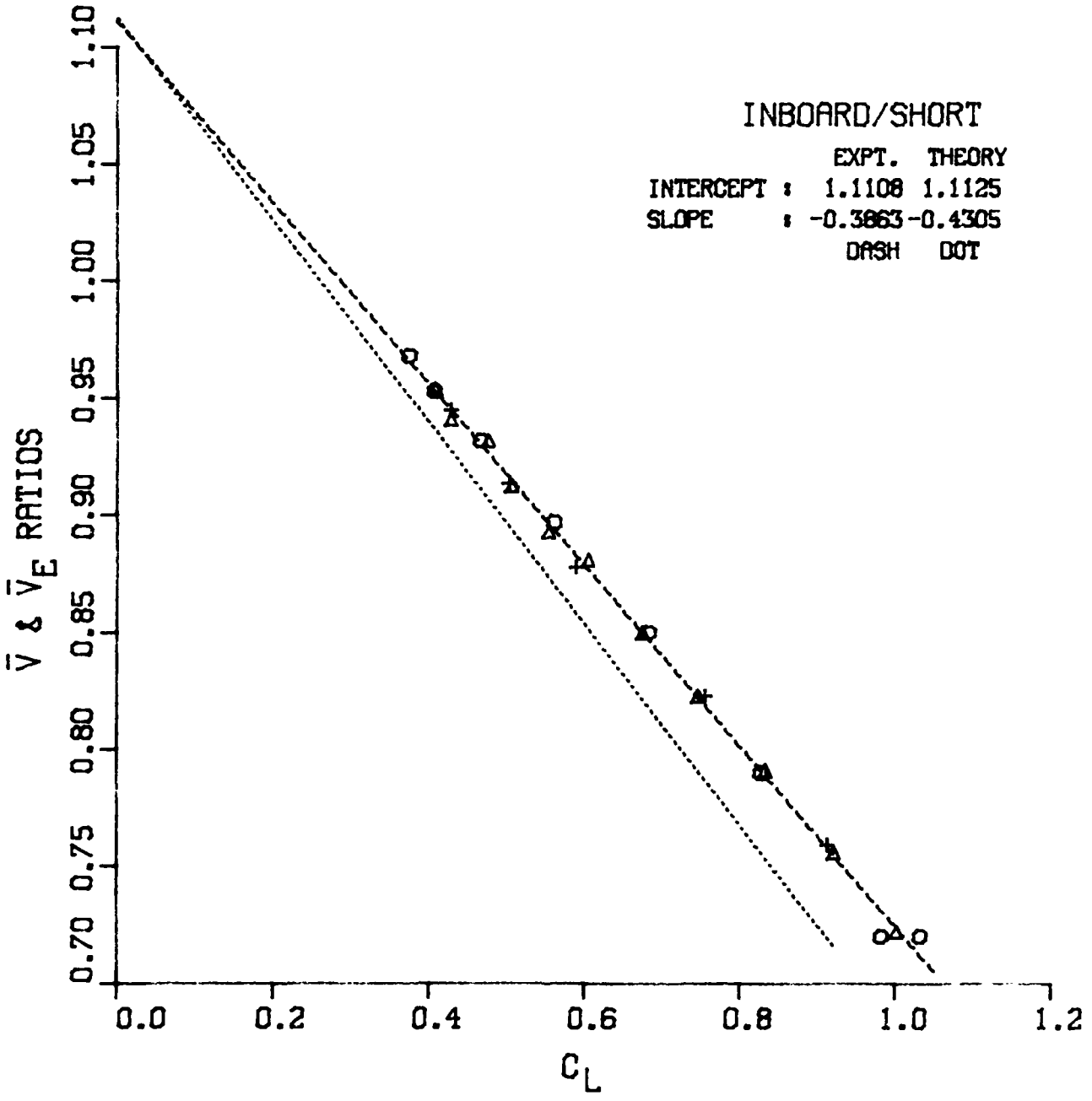

FIG. 11: VELOCITY VERSUS LIFT

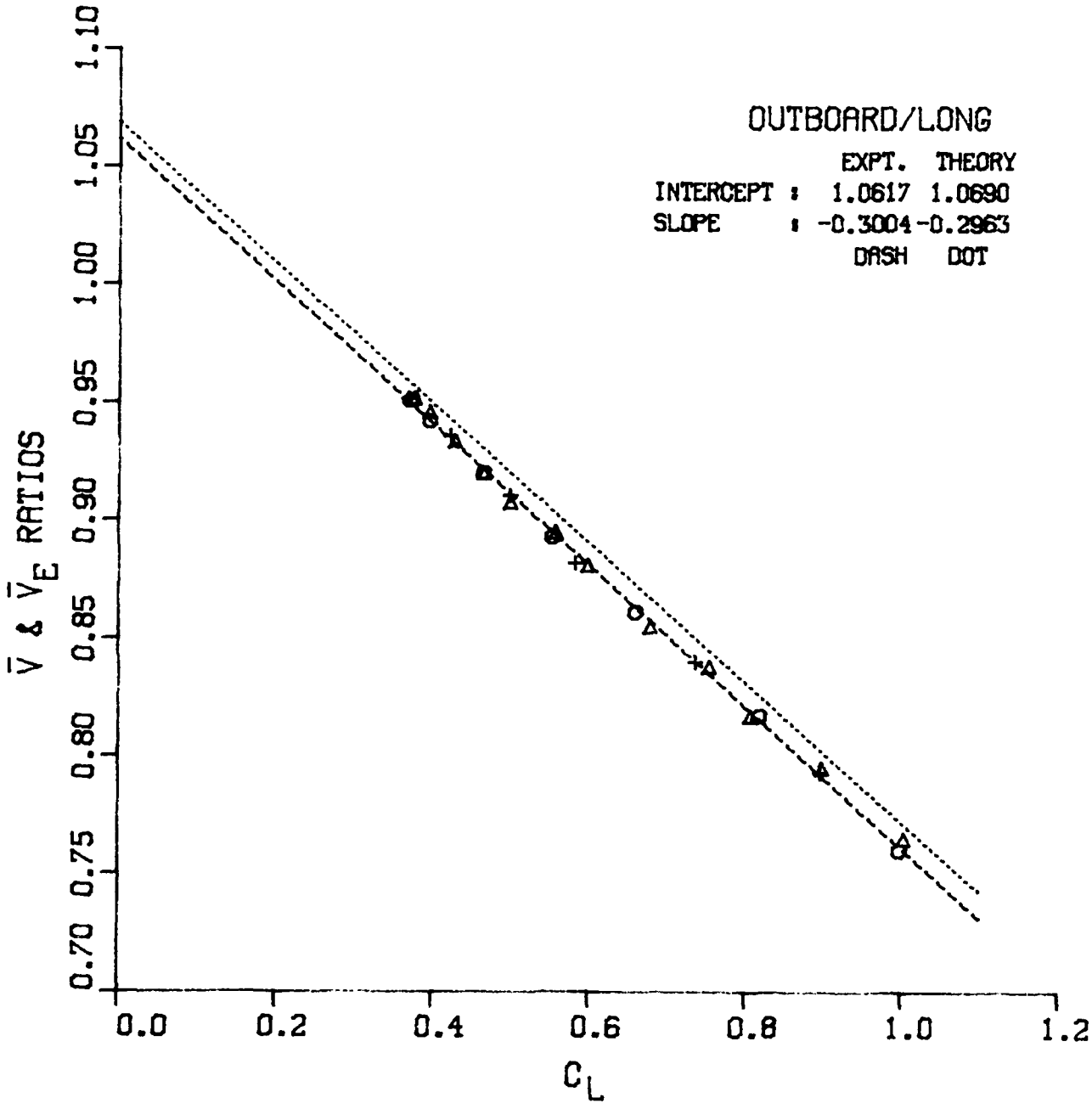

FIG. 12: VELOCITY VERSUS LIFT

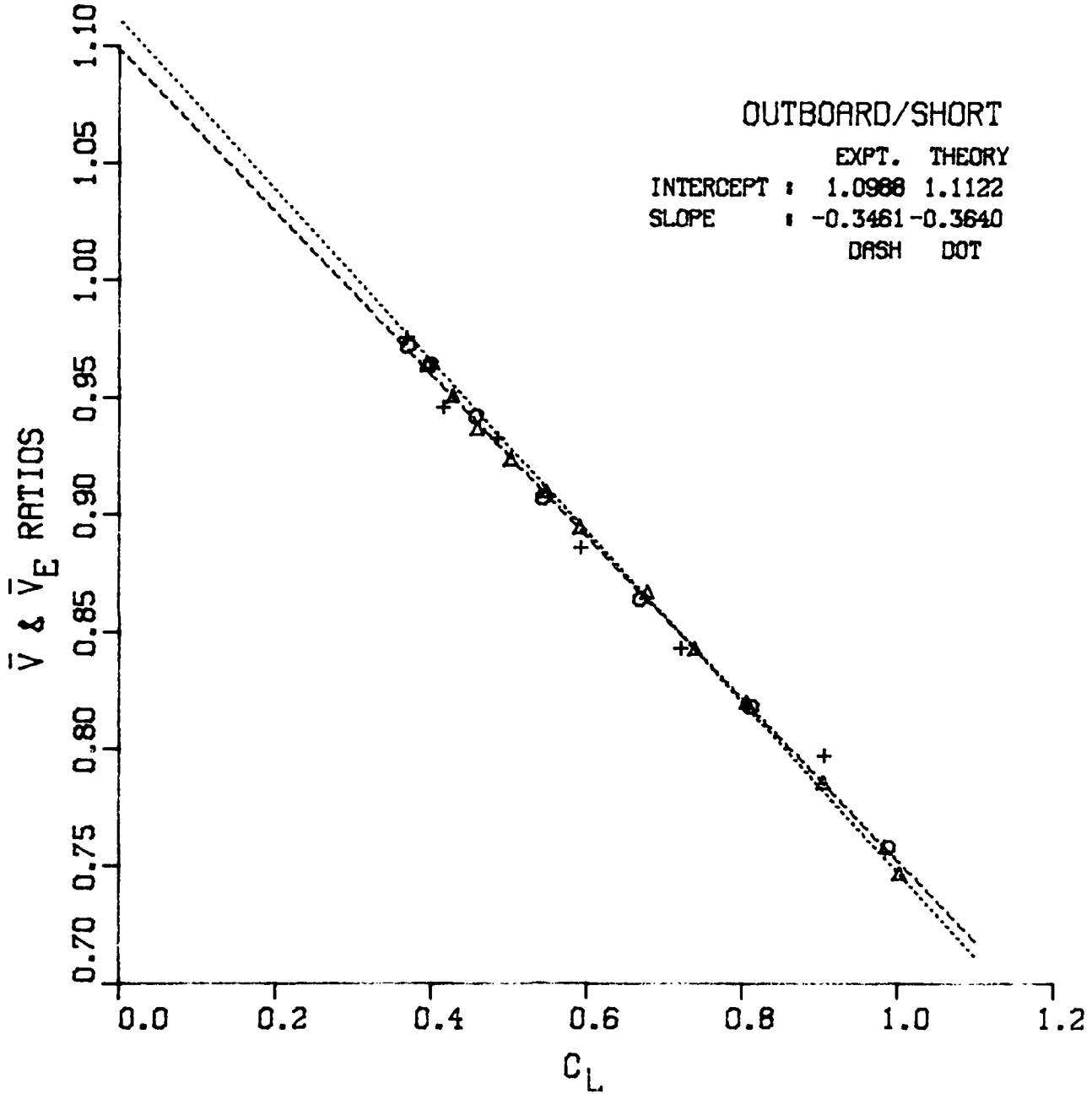

FIG. 13: VELOCITY VERSUS LIFT

APPENDIX I

A SUMMARY OF THEORY

It is not the purpose of this Appendix to re-develop the results of Glauert. However, the inclusion of a few descriptive paragraphs to introduce the concepts is thought to have merit.

A conformal transformation maps a region of one plane into another plane in such a manner that a small closed figure in one plane is mapped into a similar closed figure in another plane with a rotation and magnification (Ref. 4, p. 54). The co-ordinates in the wing plane (ζ plane) and in the transformed plane (z plane) are related by the transformation

$$\zeta = h(z) \tag{I-1}$$

The complex potential w can be defined in the z plane as:

$$w = \phi + i\,\psi\,. \tag{I-2}$$

This function is shown (Ref. 2, Section 3.3) to have its real and imaginary parts satisfy Laplace's Equation so that w may be interpreted as describing a physically possible, irrotational, two-dimensional, fluid flow.

The velocity in the z plane is

$$u - iv = \frac{dw}{dz} \tag{I-3}$$

and in the ζ plane, the velocity is $dw/d\zeta$. In terms of the flow in the z plane, the velocity in the ζ plane is

$$u_w - iv_w = (u - iv) * \frac{dz}{d\zeta} \tag{I-4}$$

where $dz/d\zeta$ is obtained from the transformation given in Equation (I-1). This point is well described by Milne-Thompson (Ref. 6, p. 66).

Normally, the flow in the z plane is known and if one can find a suitable transformation h(z), then the flow in the real (ζ) plane can be determined.

The flow around a circular cylinder of radius a with circulation Γ is (Ref. 2, p. 49)

$$w(z) = V\left(z + \frac{a^2}{z}\right) + \frac{i\Gamma}{2\pi}\,\ell n(z/a)$$

The circulation is related to the lift produced by a flow of velocity V at infinity.

The flow about a circle can be transformed into the flow around an aerofoil-like shape by substituting the variable

$$\zeta = z + \frac{a^2}{z} \tag{I-5}$$

into the expression for the flow about a circular cylinder having a radius slightly larger than a (Ref. 2, p. 50). The necessary placement of the singularities of the transformation is given in Reference 2. This result makes the general transformation in Equation (1) specific to the current problem.

The expression for the flow about a circular cylinder of radius equal to $(a + \epsilon)$ in the z plane with the flow at an angle α_o to the x axis at infinity is (Ref. 2, p. 52):

$$w = V\left[(z+\epsilon)\exp(-i\alpha_o) + \frac{(a+\epsilon)^2}{(z+\epsilon)}\exp(i\alpha_o)\right] + \frac{i\Gamma}{2\pi}\ln\left[\frac{(z+\epsilon)}{(a+\epsilon)}\exp(-i\alpha_o)\right] \tag{I-6}$$

A point ζ in the wing plane has a corresponding point z in the cylinder plane. This point can be obtained by using Equation (I-5):

$$z = \zeta/2 \pm \sqrt{(\zeta/2)^2 - a^2} \tag{I-7}$$

where the sign is chosen to make z lie outside the circle. The solution is best performed numerically because ζ and z are complex.

The velocity in the wing plane is obtained by differentiating Equation (I-6) with respect to z, calculating $dz/d\zeta$ from Equation (I-5) and substituting the results in Equation (I-4):

$$\frac{dw}{d\zeta} = \left[V\left(\exp(-i\alpha_o) - \frac{(a+\epsilon)^2}{(z+\epsilon)^2}\exp(i\alpha_o)\right) + \frac{i\Gamma}{2\pi(z+\epsilon)}\right]\left(\frac{z^2}{z^2-a^2}\right) \tag{I-8}$$

Note that this result is in terms of z. Substitution of (I-7) in (I-8) could be performed but the result for the velocity in terms of ζ is unduly cumbersome. The factor outside the square brackets comes from Equation (I-5). Equation (I-8) describes the flow about a symmetrical wing whose thickness is related to ϵ.

The Kutta Condition (Ref. 3, p. 68) is used to fix the rear stagnation point to the wing trailing edge by chosing Γ in such a way that the factor inside the square brackets in Equation (I-8) is equal to zero at z = a. The result is

$$\Gamma = 4\pi(a+\epsilon)\,V\sin\alpha_o \tag{I-9}$$

APPENDIX II

LOCATION OF PROBE SAMPLE CENTERS

Chord = 78″ a = 19.5 inches

Distance aft of leading edge: 7.90 inches $\xi/a = -1.595$

Distance below chord line: short pylon, 11.31 inches; $\eta/a = -.580$

long pylon, 15.56 inches; $\eta/a = -.798$

Position uncertainty ± 3/16″; ξ/a and $\eta/a = \pm .01$

Spanwise location: Outboard s = .747

Inboard s = .618

REPORT DOCUMENTATION PAGE / PAGE DE DOCUMENTATION DE RAPPORT

REPORT/RAPPORT	REPORT/RAPPORT
NAE-AN-19 (1a)	NRC No. 33184 (1b)
REPORT SECURITY CLASSIFICATION / CLASSIFICATION DE SÉCURITÉ DE RAPPORT	DISTRIBUTION (LIMITATIONS)
Unclassified (2)	Unlimited (3)

TITLE/SUBTITLE/TITRE/SOUS-TITRE

Theoretical and Measured Airflow About the Twin Otter Wing (4)

AUTHOR(S)/AUTEUR(S)

A.M. Drummond and J.I. MacPherson (5)

SERIES/SÉRIE

Aeronautical Note (6)

CORPORATE AUTHOR/PERFORMING AGENCY/AUTEUR D'ENTREPRISE/AGENCE D'EXÉCUTION

National Research Council Canada
National Aeronautical Establishment — Flight Research Laboratory (7)

SPONSORING AGENCY/AGENCE DE SUBVENTION

(8)

DATE	FILE/DOSSIER	LAB. ORDER / COMMANDE DU LAB.	PAGES	FIGS/DIAGRAMMES
84-03 (9)	(10)	(11)	41 (12a)	13 (12b)

NOTES

(13)

DESCRIPTORS (KEY WORDS)/MOTS-CLÉS

1. Wing theory
2. Flow (plates) — measurement
3. Air flow

(14)

SUMMARY/SOMMAIRE

The NAE Twin Otter atmospheric research aircraft carries instruments mounted under the wings to count and image cloud and precipitation particles for cloud physics studies. As part of an investigation on the influence of the aircraft presence on these measurements, airflow velocities about the wing have been calculated. These theoretical results have been compared with in-flight measurements taken by pressure probes mounted in a cannister suspended from a long and a short pylon below the wing at two spanwise locations.

The Twin Otter wing has been represented by a Joukowski aerofoil of the same maximum thickness but with a cusped trailing edge. The wing camber has been neglected but aspect ratio and planform effects have been included. The effect of the cannister was included in the comparison of theory with experiment. Use of the theory aft of the quarter chord will require experimental verification.

Both experimental and theoretical results for the local flow velocity ratio are linear functions of aircraft lift coefficient (C_L) in the range of C_L between 0.35 to 1.06. The worst discrepancy between theory and experiment in the C_L range of 0.4 to 0.6 is -2.8% to +1.1%. The results for the inboard/long pylon and outboard/short pylon have considerably less deviation.

The theory has been experimentally verified to the above accuracy and can be used to describe the spatial variation of the flow velocity ahead of the wing. Applications of the theory to the study of aircraft flow effects on cloud physics measurements can proceed with a quantifiable level of confidence.

(15)

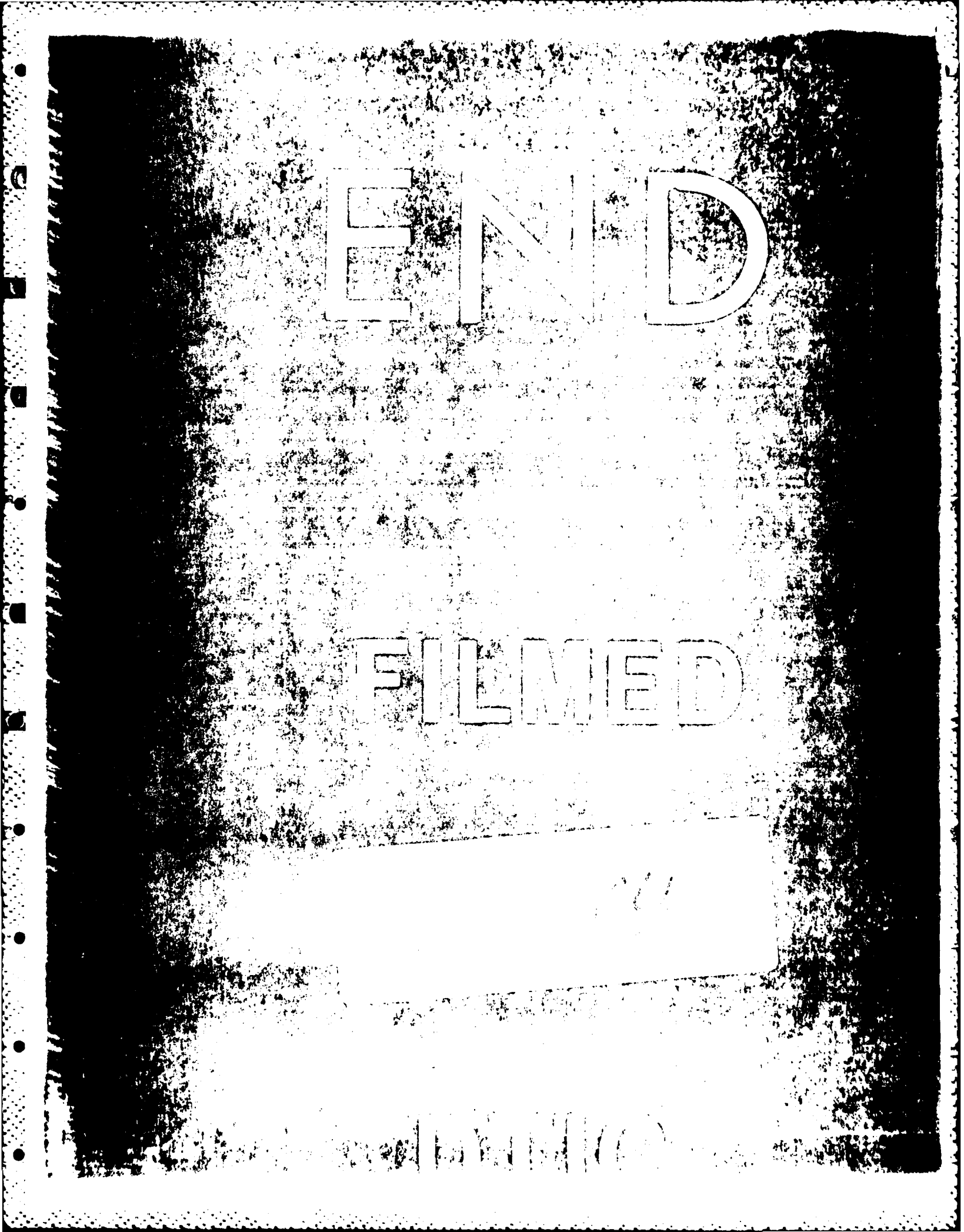
END
FILMED